12-1-2023

Do Mesopelagic Fish Biomass Patterns Change in Response to Major Oceanographic Features in the Northern Gulf of Mexico?

Ian M. Areford
Nova Southeastern University

Share Feedback About This Item

Thesis of
Ian M. Areford

Submitted in Partial Fulfillment of the Requirements for the Degree of

Master of Science
Marine Science

Nova Southeastern University
Halmos College of Arts and Sciences

December 2023

Approved:
Thesis Committee

Committee Chair: Rosanna Milligan, PhD

Committee Member: Tracey Sutton, PhD

Committee Member: Matthew Johnston, PhD

NOVA SOUTHEASTERN UNIVERSITY

HALMOS COLLEGE OF ARTS AND SCIENCES

Do Mesopelagic Fish Biomass Patterns Change in Response to Major Oceanographic Features in
the Northern Gulf of Mexico?

Ian M. Areford

Submitted to the Faculty of
Halmos College of Arts and Sciences
in partial fulfillment of the requirements for
the degree of Master of Science with a specialty in:

Marine Science

Nova Southeastern University

January 2024

Abstract

In recent years interest in mesopelagic fishes has grown due to their ecological significance and economic potential. A major outstanding question is how the assemblage is potentially structured by mesoscale (10 - 100s km) oceanographic features such as eddies, fronts, and riverine plumes. Mesoscale features are known to influence micronekton and zooplankton's spatial distributions but data on individual mesopelagic fish species' responses are limited. The Gulf of Mexico (GoM) is an area of particular interest due to its diverse mesopelagic fish assemblage, its well-defined mesoscale oceanographic features, its history of anthropogenic impacts such as oil spills, and its diverse mesopelagic fish assemblage. The most speciose group of mesopelagic fishes in the GoM is the order Stomiiformes, a hyper-diverse order that plays a major role in ecosystem functioning due to their roles as midwater predators and the trophic links they form between surface and deep-pelagic waters. The goal of this project was to determine whether mesoscale oceanographic features in the GoM such as the Loop Current, its associated eddies, and riverine plumes have a significant role in structuring the biomass distributions of Stomiiformes vertically in the water column and/or horizontally across depth strata. This project utilized Stomiiformes and oceanographic measurements obtained during the DEEPEND (Deep Pelagic Nekton Dynamics of the Gulf of Mexico) MOCNESS surveys that occurred between May 2015 – August 2018. Zero-adjusted generalized additive mixed-effects models (GAMMs) were constructed to analyze the effects of mesoscale oceanographic features on the distributions of each selected species. Most species analyzed displayed upward and/or downward shifts to their vertical distributions in response to water mass. In terms of horizontal distributions, four taxa displayed limited spatial structuring in response to distance to the 200-m isobath and/or mean monthly Chl-*a* with three displaying inverse relationships and one displaying a direct relationship. Current ecosystem models are mostly based on either abundance or acoustically derived estimates of mesopelagic fish biomass, with species-level biomass estimates rare but potentially useful. Alterations of individual mesopelagic fish species distributions have potential impacts on carbon sequestration that need to be considered in future ecosystem modeling and management efforts.

Acknowledgements

First and foremost, I would like to thank my major advisor Dr. Rosanna Milligan for all your support, encouragement, and guidance during my time at NSU and during the course of this project that ultimately made this all possible. Next, I would like to thank Dr. Tracey Sutton for allowing me access to your lab to bake the DEEPEND specimens I used during this project and for all your helpful comments and insights. I would also like to thank Dr. Matthew Johnston for your thoughtful comments on my writing, especially in regard to water mass classification, and for your insights into that process.

I want to thank all of my past and present Seascape Ecology Lab members for all the support and laughs during the course of this project and for putting up with me for the last 2 years. I would also like to thank Hannah Johnson for all the help with oven and with acquiring all of the preserved specimens I used during the project. Also, all the laughs in the lab with you and Travis were much appreciated. Finally, I want to thank all of my family and friends especially my parents for all your support and for listening to me ramble on about my project and these crazy and wacky deep-sea fish.

Table of Contents

List of Figures

List of Tables

1. Introduction

1.1. The Ecological Importance of Mesopelagic Fishes

Mesopelagic fishes inhabit the mesopelagic zone of the oceans (200 – 1000 m) which lies between the epipelagic (0 – 200 m) and the bathypelagic zones (1000 – 4000 m; Sutton, 2013). Mesopelagic fishes have the largest biomass of all marine vertebrates, with recent studies estimating their total biomass in excess of 11 billion tons (Irigoien et al., 2014). As such, mesopelagic fishes play significant roles in ecosystem functioning due to the trophic links they form between primary consumers and megafauna such as tuna, swordfish, and various marine mammals (Saunders et al., 2019). Additionally, many mesopelagic fishes display diel vertical migration (DVM) behaviors, where mesopelagic fishes migrate into the epipelagic zone to feed at dusk and then return to depth at dawn (Staby & Salvanes, 2019). DVM allows mesopelagic fishes access to the resource-rich epipelagic zone while simultaneously decreasing their predation risk (Staby & Salvanes, 2019). DVM is the largest migration (by biomass) on the planet, and it plays a critical role in the sequestration of carbon via the biological carbon pump (Davison et al., 2013). Recent model estimates put the annual flux of carbon by mesopelagic fishes at 1.5 ± 1.2 Pg C yr^{-1} with estimates highly variable primarily due to uncertainties in the estimation of biomass and metabolic rates (Saba et al., 2021). Commercially, mesopelagic fishes have been viewed as a potentially harvestable resource since the 1970s (Gjøsæter & Kawaguchi, 1980). While some species have been investigated for human consumption, the primary interest has been from the fish meal and oil industries (Turchini et al., 2010). Recently, due to growing demands for aquacultural feed and marine omega-3s, interest in potential mesopelagic fisheries has grown (Grimaldo et al., 2020). Although, mesopelagic fisheries have the potential to yield substantial amounts of proteins and omega-3s, impacts on critical ecosystem services are largely unknown due to knowledge gaps in the ecology (e.g., composition, diversity, and distribution) of the mesopelagic fish assemblage (Hidalgo & Browman, 2019).

One major question that has been identified in terms of both mesopelagic fishes' ecological importance and potential commercial viability is how the mesopelagic fish assemblage is structured in the World Ocean (St. John et al., 2016). Mesopelagic fishes' biomass distributions vary widely across global and local (1 – 10s km) scales based on oxygen content (Klevjer et al., 2016; Song et al., 2022), salinity (Wang et al., 2014), temperature (Fennell & Rose, 2015), surface

productivity (Proud et al., 2017) and solar light intensity (Aksnes et al., 2017). Additionally, mesoscale oceanographic features (e.g., eddies and fronts) through the alteration of these abiotic and biotic variables are also known to influence mesopelagic fish biomass patterns (Boswell et al., 2020; Godø et al., 2012; Herring, 2010). Mesoscale oceanographic features refer to oceanographic features that operate on spatial scales of 10s to 100s of kilometers and temporal scales of days to months and are known to create regions of physical and biological heterogeneity in the seemingly homogeneous pelagic zone of the World Ocean (Bakun, 2006). Given the prevalence of mesoscale oceanographic features and their known impact on physical and biological systems the question of whether these features influence mesopelagic fish assemblages has been asked (St. John et al., 2016). An area of particular interest in this regard is the Gulf of Mexico (GoM) due to its diverse mesopelagic fish assemblage, its well-defined mesoscale oceanographic features (Loop Current, eddies, frontal regions, etc.), and its history of anthropogenic impacts (e.g., oil spills and nutrient runoff; Sutton, Clark, et al., 2017; Sutton et al., 2020).

1.2. The Gulf of Mexico's Mesopelagic Fish Assemblage and Oceanographic Overview

The GoM is a semi-enclosed and semi-tropical ocean basin that is connected to the Caribbean Sea via the Yucatan Channel and to the northern Atlantic Ocean through the Straits of Florida. The GoM contains a unique mesopelagic fish assemblage that is characterized by greater mesopelagic fish abundances, biomass, and richness than the adjacent Caribbean and Sargasso Seas which supports the GoM's status as a unique biogeographic ecoregion in terms of mesopelagic fishes (Bangma & Haedrich, 2008; Sutton et al., 2017a). Recent, long-term micronekton trawl surveys have identified 897 species of fishes from the GoM to date which confirms previous findings that the GoM is one of the four most specious mesopelagic ecoregions in the World Ocean (Sutton et al., 2017; Sutton et al., 2020). Numerically, the GoM mesopelagic fish assemblage is dominated by the order Stomiiformes (particularly *Cyclothone* spp.) which make up around 75% of all deep-pelagic fishes caught and the order Myctophiformes which compose around 15% of the catch in recent surveys (Sutton et al., 2017b). The orders Stephanoberyciformes and Aulopiformes each contribute numerically more than 1% of the catch (Sutton et al., 2017b).

In terms of circulation patterns, the GoM can be divided into two distinct basins, the eastern and western GoM, that are dominated by two semi-permanent features of circulation. On the eastern side of the GoM circulation is dominated by the Loop Current system while the western side is dominated by a series of degraded anticyclonic and cyclonic eddies (Sturges et al., 2005). The Loop Current (LC), the dominant feature of the eastern GoM, is formed from warm waters entering the GoM through the Yucatan Channel from the Caribbean Sea (Sturges et al., 2005). As the current flows north towards the center of the GoM, it makes an anticyclonic (clockwise) turn before flowing south through the Straits of Florida where it becomes the primary source of the Gulf Stream (Figure 1; Sturges et al., 2005). The location of the LC can be highly variable with its northernmost extension reaching c. 28º N where it is in close proximity to the Mississippi River Delta (Vukovich, 2007). While the LC is in its northern position it will pinch off large anticyclonic eddies at irregular intervals before abruptly moving south where it takes a more direct path towards the Strait of Florida (Vukovich, 2007).
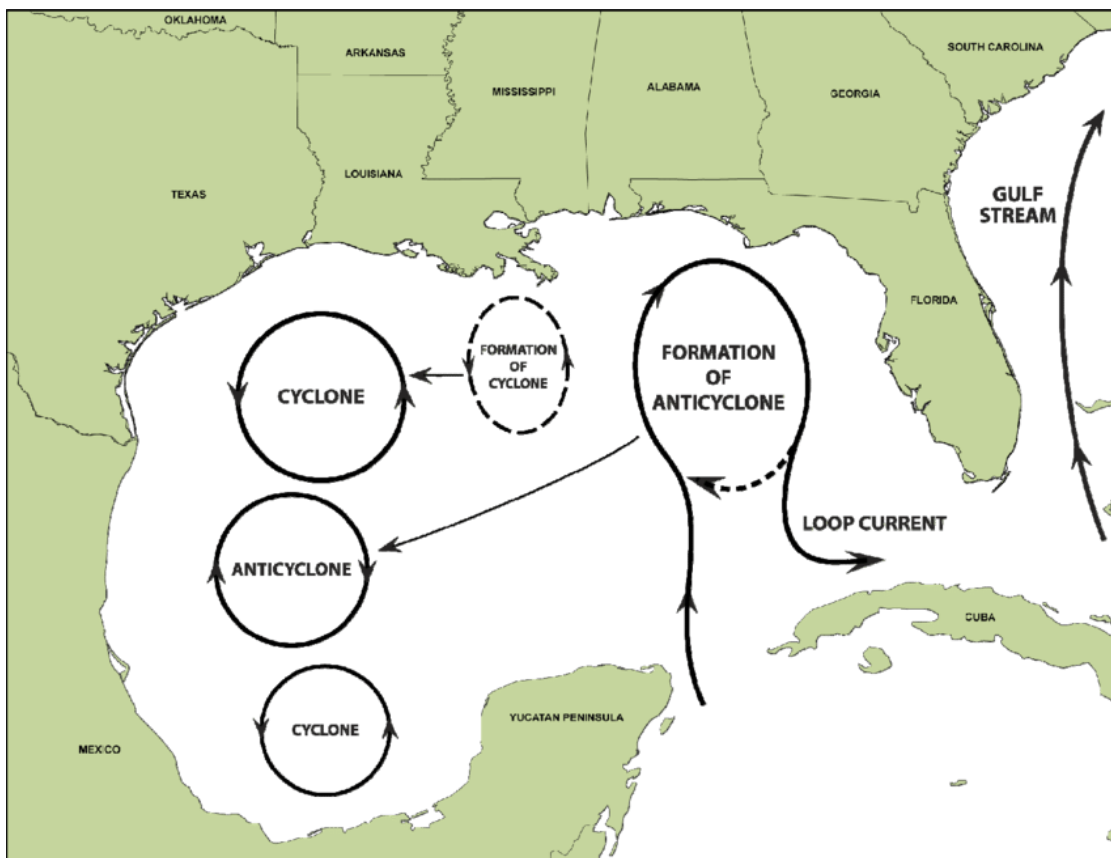
Figure 1. The Loop Current and its Associated Eddies (Grieb et al., 2008)

In addition to the LC and its associated eddies the northern GoM is also impacted by riverine input from the Mississippi River, the largest river in North America. The Mississippi River and the neighboring Atchafalaya River on average discharge over 228,600 cubic meters of water per second into the northern GoM, a rate of discharge that is only expected to increase over the course of the next century (Tao et al., 2014). Typically, the discharge is strongest during the spring (March to June) and lowest in the fall (September to November; Gierach et al., 2013). At discharge, the riverine water forms a buoyant plume that floats above the denser marine water and is typically transported westward or eastward onto the Texas or Mississippi/Alabama Shelf (Dinnel & Wiseman, 1986). As the riverine water is transported eastward during the summer it can become entrained by the LC system (Figure 2) and travel as far south as the Florida Straits (Morey et al., 2003). The large riverine discharge contains high concentrations of nutrients, specifically nitrate, which can stimulate areas of high primary productivity near shore but also offshore due to entrainment from the LC system (Dagg & Breed, 2003; Schiller et al., 2011; Vukovich, 2007).
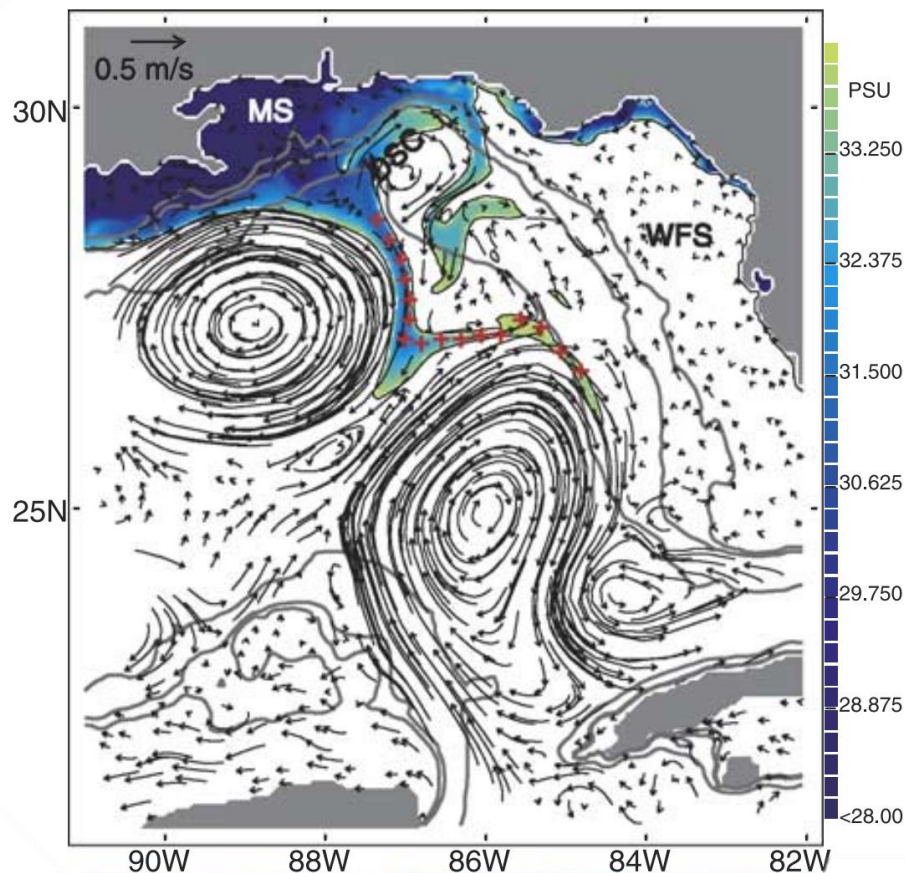
Figure 2. Low salinity Mississippi River water being entrained by the Loop Current System (Adapted from Morey et al. 2003)

1.3. Mesoscale Oceanographic Features Impacts on Horizontal Distribution Patterns of Mesopelagic Fishes

One of the main mesoscale oceanographic features in the GoM is the northern extension of the LC and its associated anticyclonic and cyclonic eddies (Figure 1; Vukovich, 2007). Large anticyclonic (clockwise) eddies often referred to as "Loop Current Eddies" (LCE) usually shed off the LC every 6 to 17 months (Maul & Vukovich, 1993) and around 45% of these separations occur between the months of March and June (Vukovich, 2007). After shedding from the LC, the newly formed LCE will propagate westwards at speeds of around $1 - 5$ km day^{-1} before eventually dissipating in the western GoM after around a year (Elliott, 1982). LCEs can reach diameters of 300 to 400 km and influence the water column to depths of up to 1500 m (Cardona & Bracco, 2016; Elliott, 1982; Zhang et al., 2023). In addition to the formation of LCEs, the eddy shedding process also involves the formation of cyclonic (anticlockwise) eddies (CE) which are the result of cold permutations that form on the western and eastern sides of the LC (Vukovich & Maul, 1985). CEs are generally small (diameters of 80 to 120 km), and they travel in the direction of LC flow (Yucatan Channel to the Florida Straits; Vukovich & Maul, 1985). CEs have been observed along the boundaries of the LC and LCEs, and usually form and intensify in the northwestern portion of the LC boundary (Vukovich, 1988). CEs are often associated with LCEs persisting on their boundary regions moving around them in a clockwise manner (Vukovich, 1988).

Generally, anticyclonic eddies are associated with convergent horizontal surface movements from the edges of the eddy towards the interior which results in downwelling conditions in the center (Figure 3b; Bakun, 2006). Due to these downwelling conditions, anticyclonic eddies are usually characterized by elevated sea surface heights, higher temperatures at depth, and lower surface productivity than surrounding water masses (Elliott, 1982; Herring, 2010; Vukovich, 2007). Due to the link between surface productivity and mesopelagic fish biomass and abundances at the global scale, it has been hypothesized that anticyclonic eddies would support lower mesopelagic fish biomass than surrounding waters (Proud et al., 2017). Cyclonic eddies are generally associated with divergent surface movements from the center of the eddy outwards which leads to upwelling conditions in the center (Figure 3a; Bakun, 2006). Due to the upwelling conditions at their centers cyclonic eddies are generally characterized by depressed sea surface heights, lower temperatures at depth, and greater surface productivity (Vukovich, 2007; Vukovich & Maul, 1985). Following the same reasoning for anticyclonic eddies it has been

hypothesized that cyclonic eddies would support greater mesopelagic fish abundances and biomass than surrounding waters (Proud et al., 2017).
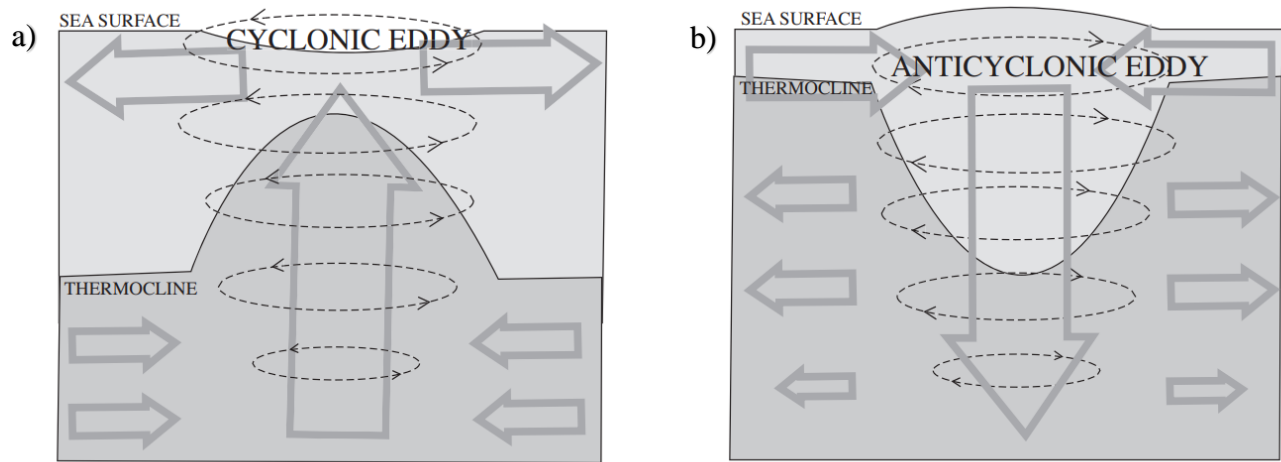
Figure 3. General circulation patterns of cyclonic and anticyclonic eddies in the Northern Hemisphere (In the Southern Hemisphere the diagram would be identical except the rotation of spin would be flipped): (a) Cyclonic Eddy, (b) Anticyclonic Eddy (Adapted from Bakun, 2006)

In terms of the mesopelagic fish assemblage, the LC and associated LCEs are generally correlated with lower acoustic backscatter (a proxy for biomass) and lower zooplankton and micronekton biomass than background GoM water, while CEs are correlated with increased acoustic backscatter and increased zooplankton and micronekton biomass than background GoM water (Boswell et al., 2020; Wormuth et al., 2000; Zimmerman & Biggs, 1999). Additionally, previous studies found that the biomass of the myctophid assemblage was significantly lower within the influence of the LC and its associated eddies (Gartner Jr et al., 1987; Wormuth et al., 2000). However, there are some limitations to these findings. For instance, many studies (e.g., Wormuth et al., 2000 and Zimmerman & Biggs, 1999) that investigated mesopelagic fish assemblages in LCEs and CEs primarily sampled the upper 350 m of the water column, which would have excluded non-migrators including many species of the numerically dominant genus *Cyclothone*. Also, acoustic data, while incredibly useful for investigating assemblage structure, lack taxonomic resolution and has the potential to underrepresent mesopelagic fish biomass due to ontogenetic changes in swim bladder morphology in certain mesopelagic fish species (Biggs & Ressler, 2001; Davison, 2011; Dornan et al., 2019).

Aside from an eddy's circulation pattern the location of eddy formation may also impact how mesopelagic fish biomass is structured within eddies. In the northern Atlantic studies found that acoustic backscatter, species richness, and the diversity of mesopelagic fishes were elevated in anticyclonic eddies rather than reduced (Della Penna & Gaube, 2020; Devine et al., 2021; Godø et al., 2012). In the Mozambique Channel, a relatively narrow channel between Africa and Madagascar, a more complex situation was presented with both anticyclonic and cyclonic eddies hosting greater acoustic backscatter depending on the sampled year (Béhagle et al., 2014; Sabarros et al., 2009). One characteristic of anticyclonic eddies that results from their horizontal movements is that they will often entrain the waters in which they form and transport those waters to new locations (Bakun, 2006). This can result in anticyclonic eddies entraining more productive water masses at their cores which could "prime" the eddy with a more productive ecosystem (Della Penna & Gaube, 2020). In the northern Atlantic studies, the sampled anticyclonic eddies were observed to have originated in more productive coastal waters and showed distinctive trapping of near-surface Chl-*a* which was hypothesized to have contributed to greater acoustic backscatter (Della Penna & Gaube, 2020; Godø et al., 2012). In the relatively narrow Mozambique Channel anticyclonic eddies are known to entrain nearshore nutrients and phyto- and zooplankton which was also hypothesized to have contributed to greater mesopelagic fish biomass in the sampled anticyclonic eddy (Béhagle et al., 2014; Sabarros et al., 2009). However, in the GoM LCEs despite their proximity to the Mississippi River are characterized by similar oceanographic conditions as the LC (e.g., nutrient depleted and low Chl-*a*; Biggs, 1992), and so LCEs are unlikely to be "primed" with more productive ecosystems due to their formation within the LC.

Located at the periphery of the LC and its associated eddies are frontal boundaries which are defined as the gradient between two water mass types. In the northern GoM, frontal boundary regions (much like other boundary regions around the world) are known to concentrate and attract prey for upper trophic level predators and are known as regions of high larval fish diversity and biomass (Lindo-Atichati et al., 2012; Mohan et al., 2017; Richards et al., 1993). Frontal boundary regions associated with the LC and its LCEs are also areas of enhanced vertical mixing due to high levels of vertical shear (Biggs & Ressler, 2001). These areas of enhanced vertical mixing have the potential to create anomalously high nutrient concentrations which can lead to "halos" of locally high Chl-*a* concentrations around the periphery of LCEs (Biggs & Ressler, 2001). Additionally, Boswell et al. (2020) demonstrated that there is an increase in acoustic backscatter in frontal

boundaries in comparison to LC waters but less backscatter when compared to Gulf Common Waters, suggesting that the frontal boundary regions in terms of biomass were an intermediate between Gulf Common Waters and the Loop Current Origin Waters. However, it should be noted that the highest single acoustic backscatter signature in Boswell et al. (2020) occurred at night within a frontal boundary station. This could mean that mesopelagic fish biomass within the frontal boundaries may be particularly patchy with areas of both high and low biomass which could be due to the dynamic and transient nature of frontal boundary regions.

Coastal influences from the Mississippi River have also been known to potentially structure various fish assemblages in the northern GoM. For instance, larval fishes have been found to partition their habitat (Pruzinsky et al., 2020; Rooker et al., 2012), with certain species of tuna (e.g., *Euthynnus alletteratus and Auxis thazard*) and billfish (e.g., *Istiophorus platypterus)* primarily associated with nearshore regions (low salinity / high productivity) and others (e.g., *Thunnus atlanticus*) primarily inhabiting offshore regions (high salinity / lower productivity; Pruzinsky et al., 2020; Rooker et al., 2012). Additionally, a study of the northern GoM larval fish assemblage collected in the upper 100 m found that areas of lower surface salinity were associated with areas of increased diversity (Meinert et al., 2020). However, when the larvae of mesopelagic fishes were isolated from the entire larval assemblage, limited horizontal structuring was found in the presence of the lower salinity Mississippi River plume (Wang et al., 2021). Additionally, a study that investigated the adult myctophid assemblage in the northern GoM through 2011 found limited horizontal structuring despite the presence of the plume (Milligan & Sutton, 2020). It is worth noting that the effects of the Mississippi River plume have primarily been investigated in relation to nearshore taxa and fish larvae with few studies on the potential impacts on offshore species and specifically the mesopelagic fish assemblage in terms of biomass. However, localized highly productive regions in the GoM such as CEs have been shown to support greater mesopelagic fish biomass (Zimmerman & Biggs, 1999). Considering the Mississippi River plume is known as a transient region of high primary productivity it is reasonable to expect that it could potentially support greater mesopelagic fish biomass. However, the enhancement of mesopelagic fish biomass assumes that mesopelagic fishes are able to "hold station" within the plume region for an extended period of time which has yet to be demonstrated.

1.4. Mesoscale Oceanographic Features Impacts on Vertical Distribution Patterns of Mesopelagic Fishes

Mesoscale oceanographic features can impact the vertical distributions of mesopelagic fishes. For instance, within LCEs it was noted that there was a deep accumulation of biomass in the lower mesopelagic (600 - 1,000 m) during both day and night when compared to surrounding water masses (Boswell et al., 2020). So, while there were decreases in biomass within the epipelagic and upper mesopelagic zones within LCEs this corresponded with an increase in lower mesopelagic biomass (Boswell et al., 2020). The increase in lower mesopelagic biomass suggests that simply examining the horizontal biomass distributions of mesopelagic fishes may not fully represent the entire impact that eddies have on biomass distributions. Additionally, within the LC and LCEs the center of mass of the DSL was found to be deeper during both day and night (Boswell et al., 2020). Within sampled CEs in the GoM the opposite result was found with zooplankton, nekton, and the center of mass of the DSL found higher in the water column during both day and night (Cummings, 1984; Zimmerman & Biggs, 1999). From these studies it appears that the GoM mesopelagic fish assemblage is located deeper within LCEs and shallower within CEs compared to the residual Gulf water.

In the GoM Boswell et al. (2020) suggested that the deepening of the deep scattering layer (DSL) during the day within LCEs was due to organisms remaining deeper to avoid the hydrodynamic effects (downwelling) of the LCEs. Studies in the North Atlantic that also found a depression in the DSL within the centers of the sampled anticyclonic eddies hypothesized that the "bowl shaped" depression in the DSL (Figure 4) was caused by the passive transport of lethargic mesopelagic fishes which would float along water masses of equal densities (Della Penna & Gaube, 2020; Godø et al., 2012; Kaartvedt et al., 2009). Eddy modeling has also shown that particles released at depth will gradually become distributed along isopycnals and that they will be displaced vertically by several hundred meters from where they were initially dispersed (Samuelsen et al., 2012). This rationale of passive transport could potentially explain daytime distributions in CEs as well since the isopyncals would be displaced upwards which would mean lethargic mesopelagic fishes residing along the same density water mass would in turn be displaced upwards. However, it is not clear the extent to which mesopelagic fish act as passive particles in the water column, especially with a recent study noting that *Benthosema glaciale* was more active at depth during the day than originally thought (Kaartvedt et al., 2023).
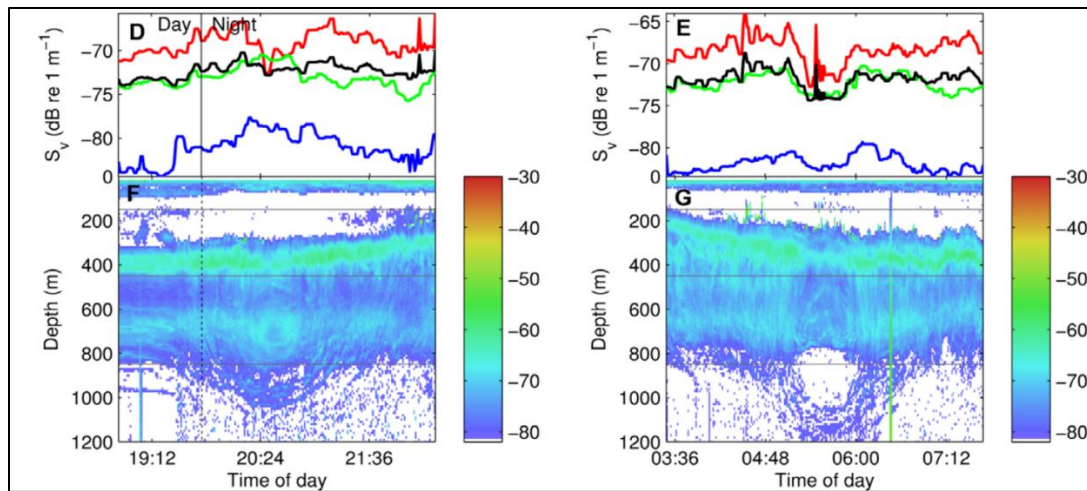
Figure 4. The "bowl shaped" depression found within the DSL of the sampled anticyclonic eddy in Northern Atlantic (Adapted from Godo et al., 2012)

Productivity has also been noted as a possible reason for the alterations in mesopelagic fishes' vertical distributions in eddies. For instance, the "doming" of the nitracline and the resulting increased productivity within sampled CEs was used to explain the upward shift in zooplankton and micronekton in the northern GoM (Wormuth et al., 2000; Zimmerman & Biggs, 1999). Additionally, zooplankton have been shown to exhibit enhanced DVM behavior in the presence of increased food availability in Sargasso Sea eddies and decreased DVM behavior in the presence of lower food availability (Eden et al., 2009; Goldthwait & Steinberg, 2008). This was also shown in micronekton off the coast of Australia where reduced DVM behavior was associated with "warm-core" eddies, which was hypothesized to be due to reduced food availability and metabolic benefits (Eden et al., 2009; Kwong et al., 2020). However, Boswell et al. (2020) noted in the GoM that the center of mass of the DSL at night and during the day correlated with surface Chl-*a* concentrations, with a deepening of the DSL with lower Chl-*a* concentrations. This would suggest another environmental driver related to productivity is influencing the vertical distributions of mesopelagic fishes since productivity alone does not adequately explain the upward or downward shifts in mesopelagic fishes' vertical distributions unrelated to DVM (daytime distributions).

Turbidity and thus light intensity may play a role in daytime vertical distributions since more productive waters increase turbidity and thus decrease light intensity at depth. Light

10

penetration is typically deeper within anticyclonic eddies due to lower productivity in the water column which results in lower turbidity (Bakun, 2006). Thus, in order for mesopelagic fishes to remain at their ideal light level (to avoid predation) they must inhabit a deeper depth (Aksnes et al., 2017). In cyclonic eddies the situation would be reversed due to increased productivity, so it would be expected that mesopelagic fishes would reside shallower in the water column. This idea would also potentially extend to other areas of high productivity and turbidity other than cyclonic eddies such as river plumes. On a global scale the light comfort zone hypothesis has support since it has been observed that light penetration depth is correlated with the depth of the DSL (Aksnes et al., 2017). Crustaceans and zooplankton that inhabit the mesopelagic zone and exhibit DVM behavior are also known to change their depth based on the intensity of light (Bandara et al., 2021; Dawidowicz & Pijanowska, 2018). Additionally, in the Southern Ocean a deepening of the DSL was also reported in association with anticyclonic eddies, with deeper light penetration noted as a possible influence (Penna et al., 2021). Light penetration has also been noted as a possible reason for depressed nighttime distributions of mesopelagic fishes in response to the lunar cycle (Drazen et al., 2011) but a reduction in DVM behavior in response to anticyclonic eddies has also been hypothesized. However, the lack of trawl data studies investigating the vertical distributions of mesopelagic fishes within the LC, LCEs, or CEs makes proving or disproving this theory within the GoM difficult since knowledge of individual taxa's DVM behavior is required.

1.5. Study Aims

The primary aim of this study is to determine whether mesoscale oceanographic features such as the Loop Current, LCEs and the Mississippi River plume significantly affect the horizontal and/or vertical biomass distributions of six common species of mesopelagic stomiiform fishes from the northern Gulf of Mexico between 2015 and 2021. The secondary aim of this study was to describe the growth forms of the six selected stomiiform fishes using their calculated length-weight parameters.

2. Methods

2.1. DEEPEND Sampling Design and Sample Processing

This project utilized mesopelagic fishes and oceanographic measurements previously obtained during the DEEPEND (Deep Pelagic Nekton Dynamics of the Gulf of Mexico) research program that occurred from May 2015 to May 2021 in the northern GoM. Each DEEPEND cruise lasted approximately 15 days and the cruises utilized in this project (DP01-DP07) occurred during May (2015-2017, 2021), July (2018), and August (2015, 2016, 2018). The DEEPEND cruises were designed to target specific oceanographic features (Loop Current, eddies, and Mississippi River plume) to investigate the natural drivers of pelagic ecosystem structure (Cook et al., 2020). To address this aim, the sample sites (Figure 5) on the DEEPEND cruises were chosen to survey as many mesoscale oceanographic features (e.g., LCEs and Mississippi River plume) as possible (Cook et al., 2020). The selection of stations and the timing of sampling was done in coordination with hindcasts and forecasts from the United States Naval Research Laboratory's Hybrid Coordinate Ocean Model (HYCOM) and satellite imagery to predict the likely location of the targeted mesoscale oceanographic features (Cook et al., 2020; Johnston et al., 2019).
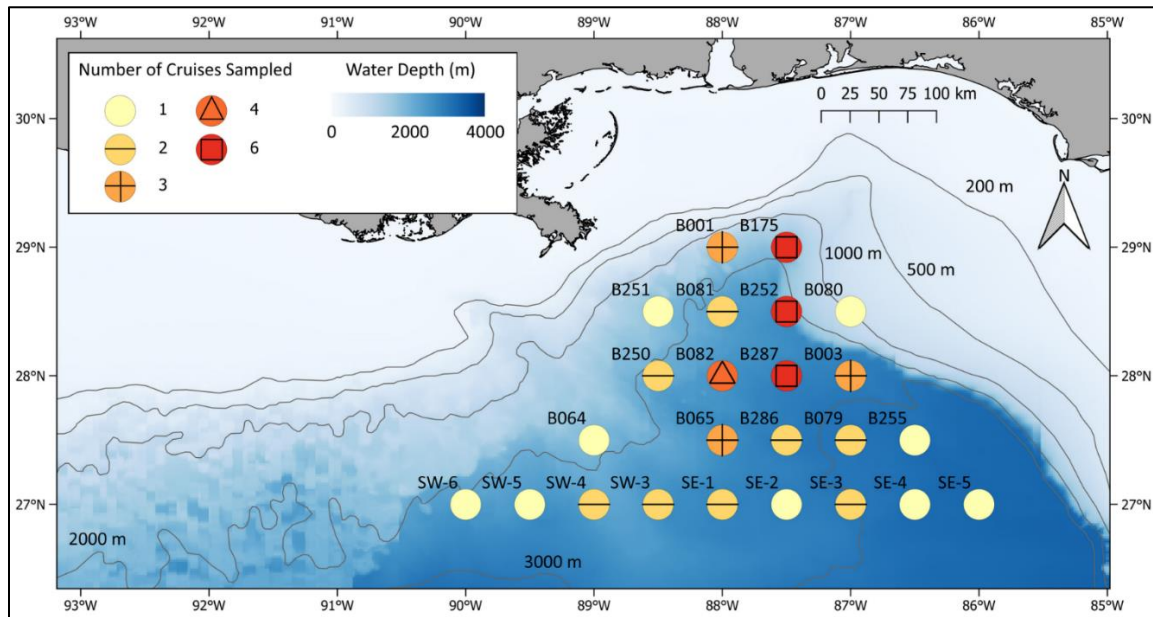
Figure 5. Sample grid and station identifications used during the DEEPEND Consortium (adapted from Cook et al. 2020)

During the DEEPEND program, micronekton were captured using a 10-m^2 Multiple Opening/Closing Net and Environmental Sensing System (MOCNESS). The deployment of the MOCNESS yielded one sample from the surface to 1500 m (downcast; not analyzed here) and five discrete-depth samples from 1500 – 1200 m (DB1), 1200 – 1000 m (DB2), 1000 – 600 m (DB3), 600 – 200 m (DB4) and 200 – 0 m (DB5) with the rationale for these depth bins following classical ecological depth zones (Sutton et al., 2013) except for DB2 which targeted the likely depth of the *Deepwater Horizon* oil spill. Sampling occurred during the day (centered around noon) and at night (centered around midnight) to examine faunal depth distributions and DVM behaviors (Cook et al., 2020). Once captured, fishes were roughly sorted by taxon and then identified to the lowest possible taxonomic level (Cook et al., 2020). Identified fishes were then counted and weighted, when possible, to the nearest gram using a motion-compensated balance (Cook et al., 2020). If the fishes did not register on the shipboard scale their weight was listed as blank (~ 68% of collected specimens). The captured fishes were then preserved with ethanol or formalin (depending on their destination) and brought back to the lab where they are currently stored (Cook et al., 2020).

2.2. Species Selection and Biomass Estimation

2.2.1 Species Selection

To examine the potential impacts of mesoscale oceanographic features on the biomass distribution patterns of stomiiform fishes in the northern GoM six species; *Cyclothone pallida*, *Cyclothone pseudopallida*, *Sigmops elongatus*, *Chauliodus sloani*, *Photostomias guernei*, and *Stomias affinis* were selected to be modeled. These six species were selected due to their high abundance within the northern GoM, their diversity of DVM behaviors and depth ranges, and specimen availability.

Table 1: Stomiiform fishes examined in study. Size ranges represent the measurement of fishes collected during DEEPEND. M = Mesopelagic zone and B = Bathypelagic zone (Data collected from Sutton et al., 2020; R. Milligan, unpublished data).

Species	Size Range (SL)	Daytime Depth	Primary Habitat	DVM Type
Cyclothone pallida	11 – 60 mm	200 - 1200 m	M/B	Non-migrator
Cyclothone pseudopallida	16 – 53 mm	200 - 1000 m	M/B	Non-migrator
Sigmops elongatus	14 – 322 mm	200 - 1000 m	M	Partial migrator
Chauliodus sloani	10 – 242 mm	200 - 1000 m	M	Partial migrator
Photostomias guernei	34 – 120 mm	200 – 600 m	M	Partial migrator
Stomias affinis	15 – 180 mm	200 – 600 m	M	Partial migrator

2.2.2 Biomass Estimation Procedure

Estimating the biomass of the mesopelagic fishes caught during the DEEPEND survey was confounded by several issues. Due to the small size of the fishes, most species did not register a weight on the motion-compensated balance, even though individuals were weighed in bulk per species. Simply reweighing all preserved specimens on shore was not an option due to the extremely large number of individuals and the distribution/destruction of specimens for other projects. As a result, to obtain a consistent and unbiased biomass estimation a modified version of the biomass estimation methodology used in Sutton and Hopkins (1996) was utilized.

The estimation of individual species biomass was conducted in a two-step process which first involved obtaining each species' individual length-weight parameters from the available preserved specimens. Estimation of individual length-weight parameters began by first selecting 20 to 50 preserved specimens from each species as recommended in Froese (2006). The selected preserved specimens were chosen to include as large a size range as possible for each species and specimens that had noticeably distended stomachs were excluded. Next each specimen's standard length (SL) was taken to the nearest 0.1 millimeters using calipers and their wet weight (WW) was determined (nearest 0.001 g). Specimens were then baked in pre-weighed aluminum weigh boats at 50º C until a constant dry weight was obtained (around 48 – 72 hours). The baked specimens

were then weighed to the nearest 0.001 g to determine their dry weight (DW). DWs were used instead of WWs in the biomass calculation process to avoid potential differences in water loss caused by preservatives and to eliminate complications due to "blotting" time and exposure to air which have been found to influence wet weights by up to 25% (Jonasson, 1972). Additionally, DW has uses in various ecological modeling applications such as carbon export models or ecosystem-based models (Woodstock et al., 2022). However, WWs were used in comparisons to other studies that calculated LWRs as it was the most common weight type used.

Once the SLs, DWs, and WWs were determined individual length-weight parameters were estimated using the logarithmic form of the equation: $W = aSL^b$, where W is either wet or dry weight (g), SL is standard length (cm), *a* is the initial growth index (the intercept), and *b* is the allometric growth coefficient (the slope; Froese 2006). The initial growth index (*a*) and the allometric growth coefficient (*b*) were then estimated using a simple linear regression model within R software 4.3.1 (R Development Core Team, 2023). In order for the estimated parameters to be used for a taxa's biomass estimation the coefficient of determination (R^2) value of the linear model needed to be greater than 0.90 as used in López-Pérez et al. (2020).

The second step of the biomass estimation process involved applying the estimated length-weight (SL – DW) parameters to the available length data. While the length data collected during the DEEPEND cruises is fairly complete, only a maximum of 25 individuals were measured at sea per species, per net sample (to the nearest mm, Cook et al., 2020). Thus, nets that contained more than 25 individuals for a species included individuals that were not measured. This meant that the length-weight parameters could not be applied directly to all the length data. So, for those net samples that included more than 25 individuals the geometric mean of the SL of that sample was used to calculate the dry weight for the unaccounted-for specimens. For those net samples that included all SLs (net samples with 25 or fewer individuals), the length-weight parameters were applied directly, and the dry weights were calculated. The total dry weight per net sample was then prorated by the volume of water filtered to obtain the final dry weight biomass estimate.

It is worth noting that while the SLs collected during the DEEPEND program were from fresh fish and the SLs used to calculate the length-weight parameters were from preserved specimens the SLs should be comparable. This is because while some studies have reported potential SL losses of around 1-3% due to preservation in ethanol this is believed to be caused by

the distortion of specimens rather than by the physical loss of SL (Kristoffersen and Salvanes, 1998). For this reason, highly distorted specimens were omitted in the specimen selection process.

2.3. Environmental Variables and Data Filtering

Biomass distribution models for the six species of interest were modelled against several environmental variables. The environmental variables (Table 2) considered included distance to nearest 200-m isobaths (representing coastal influences), minimum surface salinity (representing riverine influence), mean monthly Chlorophyll-*a* (Chl-*a*) concentration (surface productivity and riverine influence), water mass type (following Johnson et al., 2019), depth bin, and diel cycle (day/night). The water mass types were Gulf Common Water (CW), Anti-Cyclonic Ring Water (AR), mixed type (MIX), and Mississippi River plume water (RW). Distance to nearest 200 m isobath was obtained from the DEEPEND dataset and was previously calculated using the General Bathymetric Chart of the Ocean (GEBCO). Minimum surface salinity was measured via *in situ* MOCNESS sensors and was obtained from the DEEPEND Dataset (Cook et al., 2020). Mean monthly Chl-*a* was previously determined by analyzing satellite images from the Moderate Resolution Imaging Spectroradiometer (MODIS) satellite data and was obtained from the DEEPEND dataset (Cook et al., 2020). "CW", "AR", and "MIX" water mass types were identified previously based on the mean recorded temperature between 200 and 600 m depths and visual analysis of temperature-salinity profiles using data from the *in situ* MOCNESS sensors (Johnston et al., 2019). The "RW" water mass type was classified here using the minimum recorded surface salinity, with stations having surface salinities of less than 34 PSU being classified as "RW" following Morey et al. (2003).

Since depth bin was included as an explanatory variable, samples collected during the downcast (Net 0) were excluded from the analysis since it was a single oblique sample. However, preserved specimens caught in downcast samples were still used for the estimation of the length-weight parameters. Additionally, each species was represented by a "day" and "night" model to account for differences in depth ranges and response to the selected environmental variables due to diel cycle. Deployment was added as a random effect to each model to account for a lack of independence between successive depth bins samples.

Table 2. Chosen environmental variables and their possible interpretations (adapted from Milligan and Sutton 2020)

Variable (Unit)	Indication of …	Source
Distance to 200-m Isobath (kms)	Coastal Influences	General Bathymetric Chart of the Oceans (GEBCO), http://www.gebco.net
Minimum Surface Salinity (PSU)	Riverine Influence	*In situ* MOCNESS sensors
Mean Monthly Chl-*a* Concentration (mg m^{-3})	Surface Productivity and Riverine Influence	Nasa Goddard Space Flight Center, Ocean Ecology Laboratory, Ocean Biology Processing Group (2021)
Water Mass Type (CW, AR, MIX, RW)	LC, LCEs, Frontal Boundaries, and Riverine Influence	*In situ* MOCNESS sensors in accordance with Johnston et al. (2019) and Morey et al. (2003)
Depth Bin (DB1, DB2, DB3, DB4, DB5)	Vertical Distribution	*In situ* MOCNESS sensors

2.4. Presence-Absence and Biomass Distribution Statistical Analysis

2.4.1. Zero-Adjusted GAMLSS Models

The biomass distribution data were analyzed in R 4.3.1 (R Development Core Team, 2022) using "Generalized Additive Models for Location, Scale and Shape" (GAMLSS) utilizing the R package *gamlss* (Rigby & Stasinopoulos, 2005). GAMLSS models differ from traditional generalized linear model (GLMs) and generalized additive models (GAMs) in their ability to model location (e.g., mean), scale (e.g., variance), and shape (skewness and kurtosis) parameters of a chosen distribution as nonlinear functions of the predictors (Rigby & Stasinopoulos, 2005). GAMLSS models' ability to model distribution parameters allows for increased flexibility in the model fitting process and allows a user to examine potential divers of the various scale and shape parameters independently from the location parameter (e.g., mean biomass; Rigby & Stasinopoulos, 2005). Like GAMMs, GAMLSS models have the ability to allow for non-linear relationships between a response variable and multiple explanatory variables and are able to accommodate simple random effects (Rigby & Stasinopoulos, 2005).

An inherent problem with analyzing biomass-sampling data, particularly down to the species level, is the presence of zeros. This is because sampling usually yields some proportion of

zeros where the species being examined were simply not captured in a particular sample (e.g., trawl, trap, etc.). Biomass data are typically modeled using Gaussian, Log-Normal, or Gamma distributions, however the presence of zeros excludes the use of these distributions (Thorson, 2018). To combat the issue of zeros biomass-sampling data are often analyzed using zero-adjusted models which consist of two components: the probability of capturing a species and the expected biomass given that the species is present (Thorson, 2018). Due to the presence of zeroes within all the species datasets the biomass data were chosen to be modeled using zero-adjusted models.

Within the GAMLSS framework zero-adjusted models consist of a continuous and discrete portion (Figure 6; Enea et al., 2019). The continuous portion of the model includes all nonzero values of the response variable (e.g., dry weight biomass) and is modeled using any continuous distribution available in the *gamlss* package (e.g., Gamma, Gaussian, Log-Normal, etc.; Enea et al., 2019). The continuous portion of the model contains all the location, scale, and space parameters. The discrete component of the zero-adjusted model models the probability of zero/occurrence with a point mass at zero (Figure 6; Enea et al., 2019). This portion of the model is represented in the GAMLSS framework by the symbols *nu* or *xi0* (Figure 6; Enea et al., 2019). The main advantage of this framework is that it allows for both presence-absence and mean dry weight biomass to be modeled within a single model which cuts the amount of GAMLSS models that need to be fitted in half. Additionally, it allows all distribution parameters (e.g., mean biomass, variance, and occurrence) to be explained by different sets of explanatory variables.

Zero adjusted GA
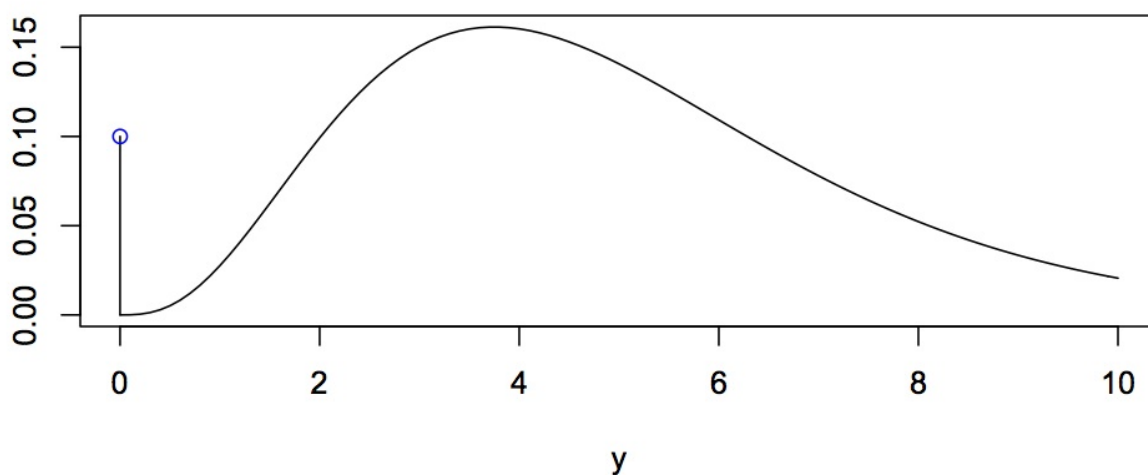
Figure 6. Visual representation of a zero adjusted gamma distribution (ZAGA) within the gamlss framework. Consists of a Gamma distribution over the continuous portion and a point mass at zero (adapted from Rigby et al., 2019)

2.4.2. Term Selection and Smoothing

Collinearity was tested before model construction to avoid possible statistical issues associated with correlation between explanatory variables (Zuur et al., 2010). Collinearity was determined by comparing the explanatory variables using pair-plots and then confirming the inclusion of variables using variance inflation factors (VIF) by sequentially dropping the covariate with the highest VIF score until the all the VIF scores were below three (Zuur et al., 2010). Due to the high level of collinearity between minimum surface salinity and water mass type, minimum surface salinity was not included in the starting ("full") models. The two remaining continuous variables (mean monthly Chl-*a* and distance to 200-m isobath) were then included in the full model using the penalized B-spline function *pb()* (Eilers & Marx, 1996; Heller et al., 2007). Penalized B-splines or "P-splines" were chosen due to their flexibility, ease of use, and their ability to shrink to a linear term if required (Eilers & Marx, 1996). The final full models before term selection were as follows:

Eq.1: Probability of Occurrence ~ Water Mass Type*Depth Bin + pb(Mean Chl-a Concentration) + pb(Distance to 200 m Isobath) + re(random = ~1| Deployment)

Eq. 2: Dry Weight Biomass Conditional on Presence ~ Water Mass Type*Depth Bin + pb(Mean Chl-a Concentration) + pb(Distance to 200 m Isobath) + re(random = ~1| Deployment)

2.4.3. Depth Bin and Water Mass Selection

Due to limited sample sizes and depth ranges all depth bins and water masses were not able to be examined for every species. Depth bins that contained less than 1% of a taxa's total abundance were removed from consideration along with water masses that included less than three trawls with collected individuals. This was to ensure the core depth ranges of the taxa were examined and that the models were able to compile as at least three samples are required to allow for a measure of its variance. Additionally, if models did not compile after depth bin and water mass selection additional depth bins or water masses were dropped until the model compiled.

2.4.4. Distribution Selection

Three distributions were considered for each species model. Two of the considered distributions, zero adjusted gamma (ZAGA) and zero adjusted inverse Gaussian (ZAIG) distributions, were considered for all species and were available in the default *gamlss* package. Both ZAGA and ZAIG distributions have previous uses in fisheries science as well as in the investigation of insurance/medical claims (Bortoluzzo et al., 2011, Di Lorenzo et al. 2022). The third distribution considered was chosen based upon fitting each individual species' non-zero dry weight biomass data with various distributions using the *FitDist* function and selecting the distribution that had the lowest corrected Akaike information criterion (AICc) score. The best fitting distribution was then constructed using the package *gamlss.inf* (Enea et al., 2019). The *gamlss.inf* package allows users to create custom zero-adjusted distributions using any of the available distributions within the *gamlss* suite of distributions (Enea et al., 2019). The other zero adjusted distributions that were considered included zero adjusted generalized gamma (GG), generalized inverse Gaussian (GIG), exponential (EXP), and Weibull (WEI; Table 3). Three full

models were then constructed using the three chosen distributions (ZAGA, ZAIG, and GG/GIG/EXP/WEI) and the final full model was chosen based on a comparison of AICc scores and the visual inspection of their residuals (Gruber, 2009). After distribution selection ten of the twelve constructed GAMMs were modeled using a ZAGA distribution and two were modeled using a zero adjusted WEI distribution (Table 3).

Table 3. AICc scores of each tested distribution. The chosen distribution is bolded. Species are represented by a three-letter code: 1) CPA = *Cyclothone pallida*; 2) CPS = *Cyclothone pseudopallida*; 3) SEL = *Sigmops elongatus*; 4) CSL = *Chauliodus sloani*; 5) PGU = *Photostomias guernei*; 6) SAF = *Stomias affinis*.

		Day			Night	
	Distribution	**AICc**	**Notes**	**Distribution**	**AICc**	**Notes**
CPA	**ZAGA**	**-211.3**	**Lowest AICc**	**ZAGA**	**-294.7**	**Lowest AICc**
	ZAIG	-116.9		ZAIG	8363	
	GIG	-183.8		GIG	-290.7	
CPS	**ZAGA**	**-208.4**	**Lowest AICc**	**ZAGA**	**-345.5**	**Lowest AICc**
	ZAIG	-91.7		ZAIG	5211.6	
	GG	-198.8		WEI	-208.3	
SEL	**ZAGA**	**94.3**	**Lowest AICc**	**ZAGA**	**219.7**	**Lowest AICc**
	ZAIG	49.2	Not Valid	ZAIG	221.9	
	GIG	99.3		GIG	261.1	
CSL	**ZAGA**	**-66.2**	**Lowest AICc**	**ZAGA**	**141.6**	**Lowest AICc**
	ZAIG	7115		ZAIG	143.1	
	GP	-	Did not compile	WEI	303.8	
PGU	ZAGA	31.1		**ZAGA**	**37**	**Lowest AICc**
	ZAIG	1431		ZAIG	47.4	
	WEI	**18.5**	**Lowest AICc**	EXP	67.8	
SAF	**ZAGA**	**18.4**	**Lowest AICc**	ZAGA	30.6	
	ZAIG	28.5		ZAIG	-25.4	Not Valid
	GIG	27.7		**WEI**	**-19.9**	**Lowest AICc**

2.4.5 Term Selection and Predicted Values

After the construction of the full models, term selection was conducted by backwards selection using the *StepGAIC* function which compared the difference between the corrected AIC scores (dAICc) of the full and reduced models. If the removal of a variable from the model resulted in a positive dAICc score, then the model fit was worsened, and that variable was retained. If the removal of a variable resulted in a negative dAICc score, then the model fit improved, and that variable was removed from the final model. This process was repeated for the mean biomass, scale parameter (variance), and presence-absence portions of the model until a minimum adequate model (MAM) was obtained. The MAM was then validated using residual and worm plots. Worm plots are detrended Q-Q plots which are constructed based on levels of the model's covariates (e.g., water mass and depth bin). This allowed for a comparison of model fit at different levels and combinations of the covariates which allowed for further refinement of the fit.

After model construction and validation, predicted mean biomasses and predicted probabilities of occurrence for each model were calculated using the function *ggpredict* within the *ggeffects* package (Lüdecke, 2018). The function *ggpredict* generates predicted values and prediction intervals which allows for the visual interpretation of complex models on the response scale (e.g., mean biomass and predicted probability of occurrence; Lüdecke, 2018). The predicted mean biomass and predicted probability of occurrence values were then used to visualize the trends between mean biomass/probability of occurrence and the final response variables for each model. For comparisons between water masses and depth bins the generated prediction intervals were used to judge significant differences between groups with no overlap indicating a significant difference. It should be noted that the function *ggpredict* generates prediction intervals based upon a Gaussian distribution so the error bars produced should be seen as approximates for all predicted mean biomass plots (Lüdecke, 2018).

3. Results

3.1. Length-Weight Regressions of Six Analyzed Stomiiformes

A total of 181 individuals belonging to two families and six species were analyzed to determine each individual species' length-weight parameters (Figure 7, Table 4). The determination coefficients (R^2) for the individual length-weight regressions were generally high (mean value of 0.945) and were all above 0.90 (Table 1). Dry weight-derived parameter *a* values ranged from 0.00036 (*Stomias affinis*) to 0.00093 (*Cyclothone pseudopallida*; Figure 7, Table 4). Dry weight-derived parameter *b* values ranged from 2.3048 (*Sigmops elongatus*) to 3.3293 (*Cyclothone pallida*; Figure 7, Table 4). Wet weight-derived parameter *a* values ranged from 0.00241 (*Stomias affinis*) to 0.00662 (*Sigmops elongatus*; Figure 7, Table 4). Wet weight-derived parameter *b* values ranged from 2.5485 (*Sigmops elongatus*) to 2.9331 (*Cyclothone pseudopallida*; Figure 7, Table 4).
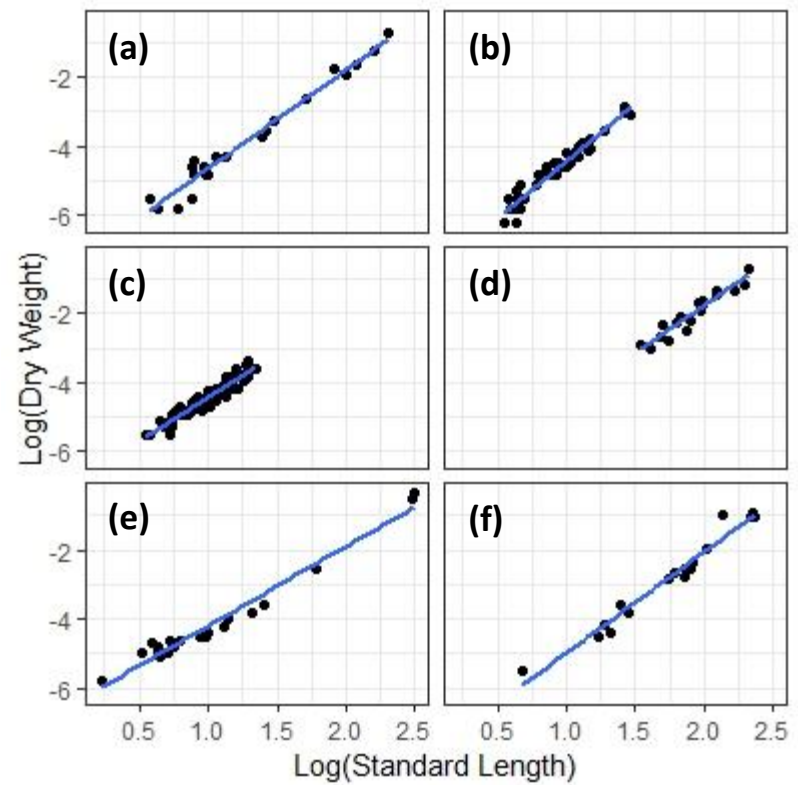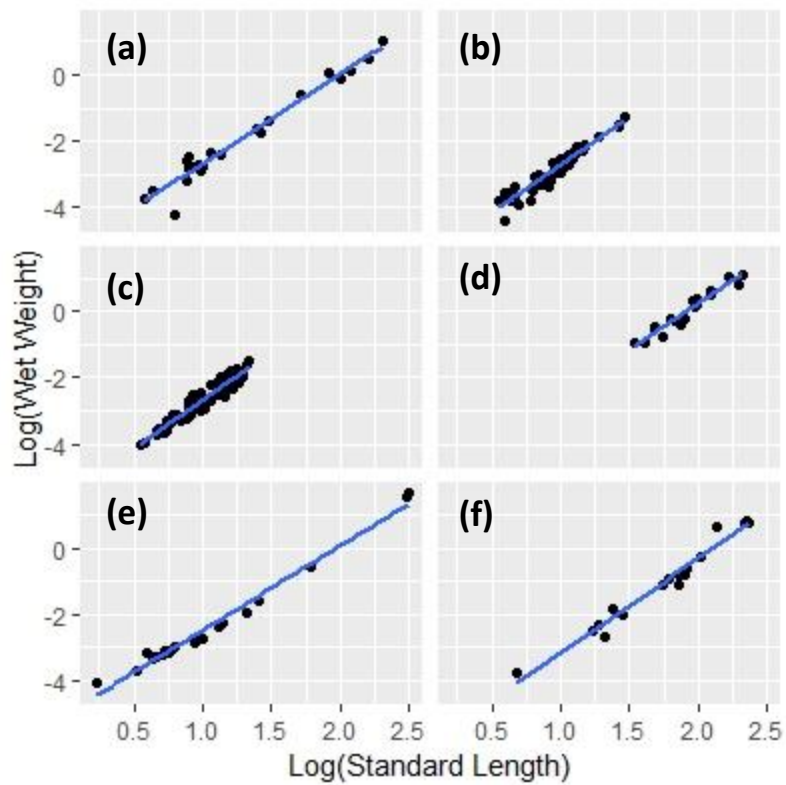
Figure 7. Length-weight regressions for the six analyzed Stomiiformes: *Chauliodus sloani* (a), *Cyclothone pallida* (b), *Cyclothone pseudopallida* (c), *Photostomias guernei* (d), *Sigmops elongatus* (e), and *Stomias affinis* (f). Wet weight length-weight regressions are in gray (left) and dry weight length-weight regressions are in white (right). Plots are on the log10 scale.

Table 4. Length-weight parameters for analyzed Stomiiformes: aWW: wet weight intercept, bWW: wet weight allometry coefficient, aDW: dry weight intercept, bDW: dry weight allometry coefficient, n: sample size, R^2: coefficient of determination, SL: standard length

Species	Size Range (SL cm)	n	aWW	bWW	R^2	aDW	bDW	R^2
Cyclothone pallida	1.58 - 4.36	46	0.00369 (0.00291, 0.00468)	2.8776 (2.6382, 3.1270)	0.923	0.00042 (0.00032, 0.00053)	3.3293 (3.0730, 3.5856)	0.940
Cyclothone pseudopallida	1.73 - 3.82	75	0.00366 (0.00292, 0.00459)	2.9331 (2.7123, 3.1538)	0.908	0.00093 (0.00077, 0.00113)	2.5314 (2.3488, 2.7140)	0.911
Sigmops elongatus	1.25 - 12.05	22	0.00662 (0.00552, 0.00795)	2.5485 (2.3919, 2.7050)	0.983	0.00077 (0.00119, 0.00188)	2.3048 (2.1962, 2.4987)	0.969
Chauliodus sloani	1.89 - 10.11	22	0.00472 (0.00332, 0.00670)	2.6921 (2.4373, 2.9462)	0.961	0.00055 (0.00040, 0.00076)	2.8507 (2.6197, 3.0816)	0.969
Photostomias guernei	4.67 - 10.15	18	0.00482 (0.00234, 0.00992)	2.7840 (2.4110, 3.1570)	0.934	0.00067 (0.00028, 0.00162)	2.7585 (2.3065, 3.2105)	0.907
Stomias affinis	1.97 - 11.13	17	0.00241 (0.00145, 0.00403)	2.8594 (2.5752, 3.1435)	0.968	0.00036 (0.00021, 0.00063)	2.9290 (2.6241, 3.2338)	0.966

3.2. Generalized Additive Mixed Model (GAMM) Results

3.2.1 *Cyclothone pallida*

3.2.1.1 *Cyclothone pallida* Presence-Absence: Data Selection

Data collected from 0 - 200 m were omitted from both day and night models due to the low number of individuals present. *Cyclothone pallida* was additionally only absent from a single 600 - 1000 m trawl sample therefore that depth bin was also excluded from both day and night full presence-absence models since a calculation of variance was unable to be obtained due to the presence of only a single zero (Table 5).

3.2.1.2 *Cyclothone pallida* Presence-Absence: Minimum Adequate Model (MAM) Results

The probability of *C. pallida* occurrence was only significantly affected by depth bin during both day and night (Figure 8, Table 6 and 7). The depth bin with the lowest predicted probability of *C. pallida* occurrence was from 1200 - 1500 m with values ranging from 74.0% during the day to 73.6% at night which was significantly lower than the other depth bin (Figure 8). The predicted probability of *C. pallida* occurrences from 1000 - 1200 m and 200 – 600 m were not significantly different from each other during both day and night with values during the day ranging from 91.8% (1000 - 1200 m) to 93.5% (200 - 600 m) and values at night ranging from 94.8% (1000 - 1200 m) to 96.3% (200 - 600 m; Figure 8). A 100% probability of occurrence was assumed for the 600 - 1000 m depth bin, in which *C. pallida* was only absent from a single daytime CW trawl sample (Figure 8).

Table 5. Summary table of modelled depth bins and water masses in full daytime and nighttime models for all modeled taxa. Includes whether the interaction term (Depth Bin x Water Mass) and the random effect (deployment) was included in full model before term selection. P/A: Presence-absence portion of model. Biomass: The mean biomass portion of model.

Species	Day				Night			
	Depth Bins	*Water Masses*	*Interaction Term*	*Random Effect*	*Depth Bins*	*Water Masses*	*Interaction Term*	*Random Effect*
C. pallida								
P/A	1, 2, 4	AR, CW, MIX, RW	Yes	Yes	1, 2, 4	AR, CW, MIX, RW	Yes	Yes
Biomass	1, 2, 3, 4	AR, CW, MIX, RW	Yes	Yes	1, 2, 3, 4	AR, CW, MIX, RW	Yes	Yes
C. pseudopallida								
P/A	3, 4	AR, CW, MIX, RW	Yes	Yes	3, 4	AR, CW, MIX, RW	Yes	Yes
Biomass	3, 4	AR, CW, MIX, RW	Yes	Yes	3, 4	AR, CW, MIX, RW	Yes	Yes
S. elongatus								
P/A	3, 4	AR, CW, RW	Yes	Yes	4, 5	AR, CW, RW	Yes	Yes
Biomass	3, 4	AR, CW, RW	Yes	Yes	4, 5	AR, CW, RW	Yes	Yes
C. sloani								
P/A	4	AR, CW, RW	No	No	4, 5	AR, CW, RW	Yes	Yes
Biomass	4	AR, CW, RW	No	No	4, 5	AR, CW, RW	Yes	Yes
P. guernei								
P/A	3	AR, CW, RW	No	No	3, 4	AR, CW	No	Yes
Biomass	3	AR, CW, RW	No	No	3, 4	AR, CW	No	Yes
S. affinis								
P/A	3, 4	CW	No	Yes	5	AR, CW	No	No
Biomass	3, 4	CW	No	Yes	5	AR, CW	No	No

Table 6. Summary table of all daytime MAM models and their retained variables after term selection. Includes a comparison of the AICc scores between full models and MAM

Species	MAM	Full Model AICc	MAM AICc
C. pallida		-101.4	-139.24
P/A	~ depth_bin + re(random = ~1 | deployment)		
Biomass	~ tpyc.class x depth_bin + re(random = ~1 | deployment)		
C. pseudopallida		-151.87	-236.29
P/A	~ tpyc.class + depth_bin + re(random = ~1 | deployment)		
Biomass	~ tpyc.class x depth_bin + re(random = ~1 | deployment)		
S. elongatus		210.72	84.18
P/A	~ pb(chla_monthly_9km) + re(random = ~1 | deployment)		
Biomass	~ tpyc.class x depth_bin + re(random = ~1 | deployment)		
C. sloani		-51.05	-72.53
P/A	~ 1		
Biomass	~ pb(chla_monthly_9km)		
P. guernei		31.08	6.01
P/A	~ pb(dist.to.200m_km)		
Biomass	~ pb(dist.to.200m_km)		
S. affinis		40.25	4.56
P/A	~ pb(chla_monthly_9km) + pb(dist.to.200m_km) + re(random = ~1 | deployment)		
Biomass	~ depth_bin + re(random = ~1 | deployment)		

Table 7. Summary table of all nighttime MAM models and their retained variables. Includes a comparison of the AICc scores between full models and MAM

Species	MAM	Full Model AICc	MAM AICc
C. pallida			
P/A	~depth_bin + re(random = ~1 | deployment)	-168.96	-222.8
Biomass	~ tpyc.class x depth_bin + re(random = ~1 | deployment)		
C. pseudopallida			
P/A	~ tpyc.class + depth_bin + re(random = ~1 | deployment)	-346.94	-350.99
Biomass	~ tpyc.class x depth_bin + re(random = ~1 | deployment)		
S. elongatus			
P/A	~ tpyc.class + depth_bin + re(random = ~1 | deployment)	180.9	108.12
Biomass	~ tpyc.class x depth_bin + re(random = ~1 | deployment)		
C. sloani			
P/A	~ tpyc.class x depth_bin + pb(dist.to.200m_km) + re(random = ~1 | deployment)	114.60	104.81
Biomass	~ tpyc.class + depth_bin + re(random = ~1 | deployment)		
P. guernei			
P/A	~ re(random = ~1 | deployment)	167.90	32.79
Biomass	~ depth_bin + re(random = ~1 | deployment)		
S. affinis			
P/A	~ 1	-13.50	-30.11
Biomass	~ pb(dist.to.200m_km)		

Figure 8. Predicted probability of *Cyclothone pallida* occurrence in relation to depth bin during day (a) and night (b).

3.2.1.3 *Cyclothone pallida* Biomass: Data Selection

For both day and night *C. pallida* mean biomass models all water masses (AR, CW, and RW) and both continuous environmental variables (monthly Chl-*a* and distance to 200-m isobath) were included in the full model (Table 5). Data collected from 0 - 200 m were omitted from both day and night models due to the low number of individuals present (Table 5).

3.2.1.4 *Cyclothone pallida* Biomass: Minimum Adequate Model (MAM) Results

Mean *C. pallida* biomass was best explained by the interaction between depth bin and water mass during both day and night (Figure 9, Table 6 and 7). Predicted mean *C. pallida* biomass during both day and night peaked at 600 – 1000 within CW (Day: 0.48 g 10^4 m^{-3}, Night: 0.41 g 10^4 m^{-3}), MIX (Day: 0.57 g 10^4 m^{-3}, Night: 0.30 g 10^4 m^{-3}), and RW (Day: 0.36 g 10^4 m^{-3}, Night: 0.34 g 10^4 m^{-3}) but within AR predicted mean biomass peaked between 1000 - 1200 m (Day: 0.44 g 10^4 m^{-3}, Night: 0.40 g 10^4 m^{-3}; Figure 9). Predicted mean *C. pallida* biomass during day and

night was lowest within the 1200 - 1500 m depth bin for CW (Day: 0.02 g 10^4 m^{-3}, Night: 0.03 g 10^4 m^{-3}), MIX (Day: 0.02 g 10^4 m^{-3}, Night: 0.02 g 10^4 m^{-3}), and RW (Day: 0.03 g 10^4 m^{-3}, Night: 0.02 g 10^4 m^{-3}), while predicted mean biomass within AR was lowest from 200 - 600 m (Day: 0.01 g 10^4 m^{-3}, Night: 0.01 g 10^4 m^{-3}; Figure 9). AR's departure from the other three water masses in these cases seems to indicate that *C. pallida* biomass is exhibiting a downward vertical shift within AR which is further supported by *C. pallida* biomass within AR being over double the amount (Day: 0.05 g 10^4 m^{-3}, Night: 0.08 g 10^4 m^{-3}) of the other water masses within the 1200 - 1500 m depth stratum (Figure 9). Additionally, the potential downward shift in *C. pallida's* vertical distribution in AR was most apparent in the nighttime model where there was a significant difference between AR and the other water masses within the 200 – 600 m, 1000 – 1200 m, and 1200 – 1500 m depth bins (Figure 9).

Another notable pattern is that while CW and RW follow similar patterns in most depth strata, RW differed from CW within the 200 - 600 m depth bin and exhibited the highest biomass of all water masses within this range during day (0.22 g 10^4 m^{-3}) and night (0.10 g 10^4 m^{-3}; Figure 9). This could potentially signify a slight upward shift in vertical distribution within RW compared to the other water masses. Additionally, this potential upward shift in *C. pallida's* vertical distribution within RW was most apparent in the daytime model where predicted mean biomass in RW was significantly higher than the other water masses within the 200 – 600 m depth bin (Figure 9).

Figure 9. Interaction plot describing the relationship between depth bin and water mass type for predicted mean biomass values of *Cyclothone pallida* during day (a) and night (b).
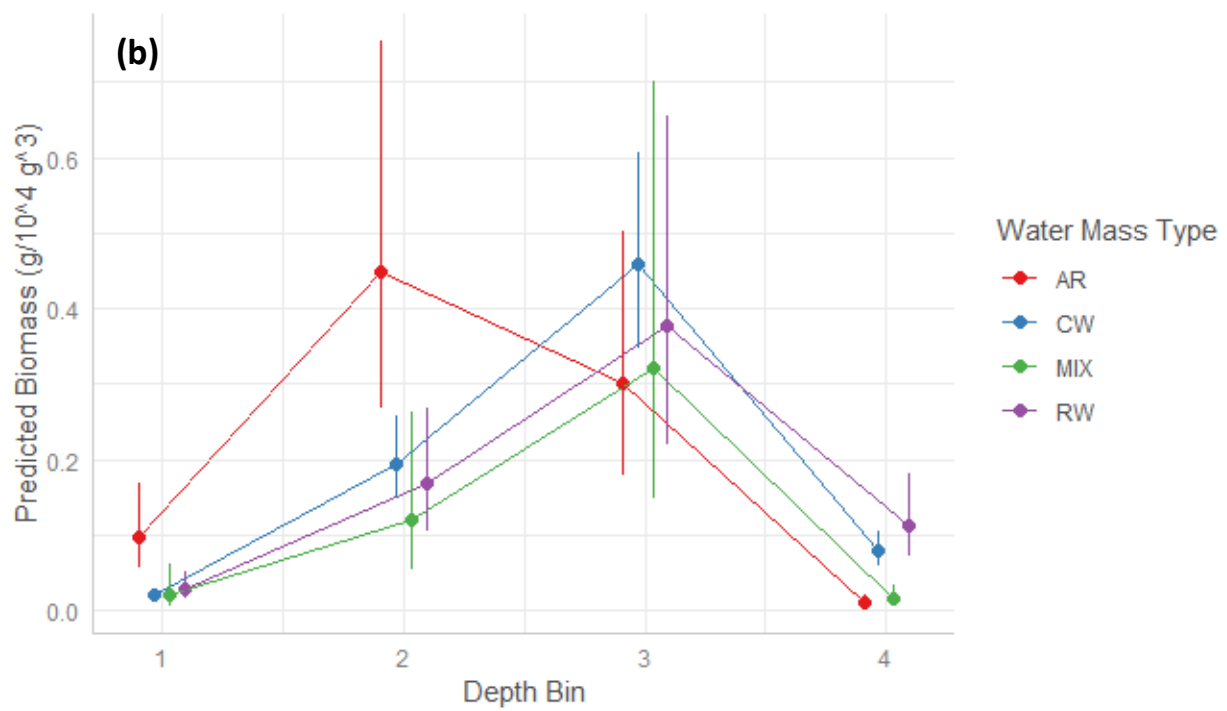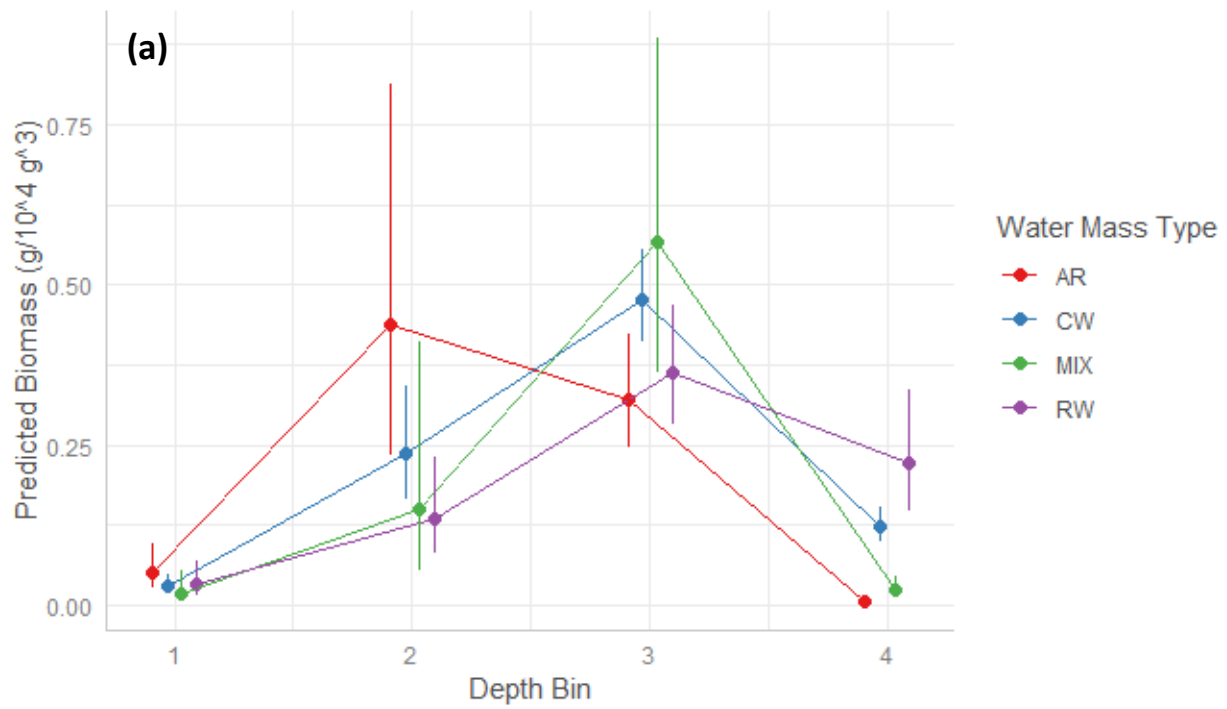
3.2.2. *Cyclothone pseudopallida*

3.2.2.1 *Cyclothone pseudopallida* Presence-Absence: Data Selection

For both day and night *C. pseudopallida* models all water masses (AR, CW, MIX, and RW) and both continuous environmental variables (monthly Chl-*a* and distance to 200-m isobath) were included in the full model (Table 5). Only data collected from 200 – 600 m and 600 – 1000 m were included in both day and night full models (Table 5). Data

3.2.2.2 *Cyclothone pseudopallida* Presence-Absence: Minimum Adequate Model (MAM) Results

The probability of *C. pseudopallida* occurrence was best explained by depth bin and water mass during both day and night (Figure 4, Table 6 and 7). The probability of *C. pseudopallida* occurrence was lowest within the 200 – 600 m depth bin during both day and night with a predicted probability of occurrence of 75% at night and 74.8% during the day (Figure 4). The predicted probability of occurrence within the 600 – 1000 m depth bin was 89.2% at night and 94% during the day (Figure 10).

During the day the water mass with the highest probability of *C. pseudopallida* occurrence was RW, with a predicted probability of occurrence of 100% (Figure 10). CW followed closely behind RW with a predicted probability of *C. pseudopallida* occurrence of 95% (Figure 10). MIX had a predicted probability of occurrence of 87% during day and AR had a predicted probability of occurrence of 56% which was the lowest value (Figure 10). During the day the differences between waters masses were all significant.

At night the water masses with the highest probability of *C. pseudopallida* occurrence were RW and CW, with predicted probabilities of occurrence of 96% and 95.5% respectfully (Figure 10). The water masses with the lowest probability of *C. pseudopallida* occurrence were MIX and AR with predicted probabilities of occurrence of 75% and 61.5% respectfully (Figure 10). CW and RW were not significantly different from each other, and both had significantly higher probabilities of *C. pseudopallida* occurrence than AR and MIX (Figure 10). The predicted probability of *C. pseudopallida* occurrence was not significantly different in AR and MIX (Figure 10).
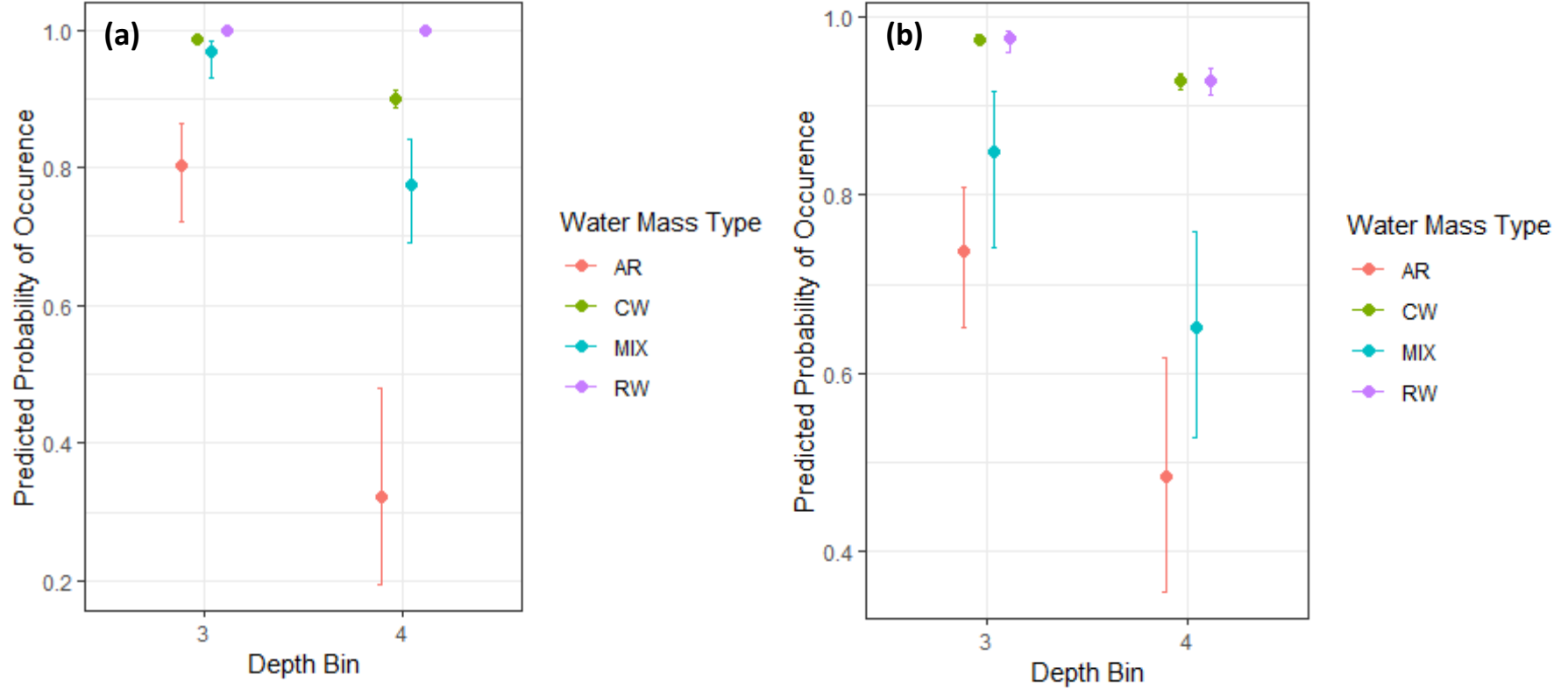
Figure 10. Predicted probability of *Cyclothone pseudopallida* occurrence during day (a) and night (b) in relation to depth bin and water mass.

3.2.2.3 *Cyclothone pseudopallida* Biomass: Data Selection

For both day and night, all water masses (AR, CW, MIX, and RW) and both continuous environmental variables (monthly Chl-*a* and distance to 200-m isobath) were included in the full models (Table 5). Only data collected from 200 - 600 m and 600 - 1000 m were included in both day and night full models due to insufficient data in the other depth bins (Table 5).

3.2.2.4 *Cyclothone pseudopallida* Biomass: Minimum Adequate Model (MAM) Results

Mean *C. pseudopallida* biomass was best explained by the interaction between depth bin and water mass during both day and night (Figure 11, Table 6 and 7). During the day within the 200 – 600 m depth bin predicted mean *C. pseudopallida* biomass was highest within RW (0.15 g 10^4 m^{-3}), CW (0.13 g 10^4 m^{-3}) and MIX (0.08 g 10^4 m^{-3}) which all had significantly higher biomass than AR (0.01 g 10^4 m^{-3}; Figure 11). Predicted mean *C. pseudopallida* biomass was not significantly different in CW, MIX, and RW within the 200 – 600 m depth bin (Figure 11). Within the 600 – 1000 m depth bin *C. pseudopallida* biomass was highest within AR (0.10 g 10^4 m^{-3}), CW (0.05 g 10^4 m^{-3}), and MIX (0.09 g 10^4 m^{-3}) which all had significantly greater predicted mean biomass than RW (0.02 g 10^4 m^{-3}; Figure 11). Predicted mean *C. pseudopallida* biomass was not significantly different in AR, CW, and MIX within the 600 –1000 m depth bin (Figure 11).

At night within the 200 – 600 m depth bin predicted mean *C. pseudopallida* biomass was significantly highest within RW (0.05 g 10^4 m^{-3}) and CW (0.06 g 10^4 m^{-3}). Predicted mean *C. pseudopallida* biomass within MIX (0.02 g 10^4 m^{-3}) was significantly higher than AR (0.01 g 10^4 m^{-3}) which possessed the lowest predicted mean biomass among the water masses within the 200 – 600 m depth bin (Figure 11). Predicted mean *C. pseudopallida* biomass within the 600 – 1000 m depth bin was highest within AR (0.07 g 10^4 m^{-3}), MIX (0.05 g 10^4 m^{-3}) and RW (0.02 g 10^4 m^{-3}; Figure 11). AR had significantly greater biomass than CW (0.05 g 10^4 m^{-3}) but MIX and RW were not significantly different than CW which had the lowest predicted mean *C. pseudopallida* biomass within the 600 – 1000 m depth bin (Figure 11).
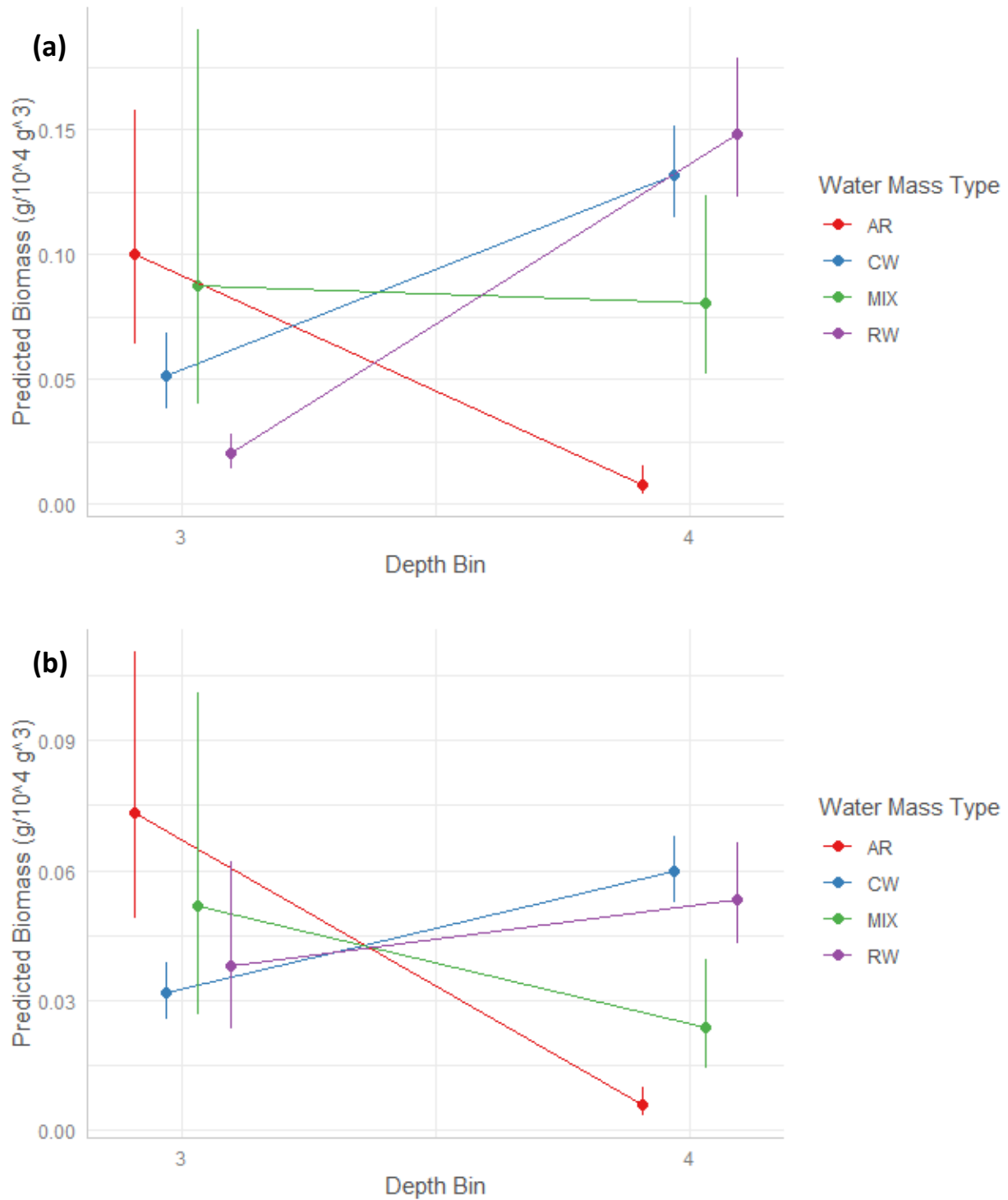
Figure 11. Interaction plot describing the relationship between depth bin and water mass type for predicted mean biomass values of *Cyclothone pseudopallida* during day (a) and night (b).

3.2.3. *Sigmops elongatus*

3.2.3.1 *Sigmops elongatus* Presence-Absence: Data Selection

For both day and night *S. elongatus* presence-absence models all water masses except for MIX (AR, CW, and RW) were included in the full models along with both continuous environmental variables (monthly Chl-*a* and distance to 200-m isobath; Table 5). In the full day presence-absence model for *S. elongatus* only data collected from 200 – 600 m and 600 – 1000 m were included in the full model and in the full night presence-absence model only data collected from 0 – 200 m and 200 – 600 m were included in the full model due to insufficient data in the other depth bins (Table 5).

3.2.3.2 *Sigmops elongatus* Presence-Absence: Minimum Adequate Model (MAM) Results

The probability of *S. elongatus* occurrence during the day was significantly affected by mean monthly Chl-*a* (Figure 5, Table 6). The relationship between predicted probability of *S. elongatus* occurrence and mean monthly Chl-*a* was roughly linear with the predicted probability of occurrence decreasing with increasing values of monthly Chl-*a* (Figure 5)*.* The predicted probability of *S. elongatus* occurrence ranged from 66% at mean monthly Chl-*a* levels of 0.05 mg m^{-3} to 16% at mean monthly Chl-*a* values of 1.38 mg/m^{-3} (Figure 5).

The probability of *S. elongatus* occurrence at night was significantly affected by depth bin and water mass type (Figure 5). Predicted probability of *S. elongatus* occurrence was highest in the 0 - 200 m depth bin with a predicted probability of occurrence of 76.6 % compared to a predicted probability of occurrence in the 200 – 600 m depth bin of 38.4 % (Figure 5). Predicted probability of *S. elongatus* occurrence was significantly higher in CW (70 %) compared to AR (55.5 %) and then RW (47 %) across depth bins. Predicted probability of *S. elongatus* occurrence was significantly higher in AR compared to RW in the 0 - 200 m depth bin but they were not significantly different in the 200 – 600 m depth bin.

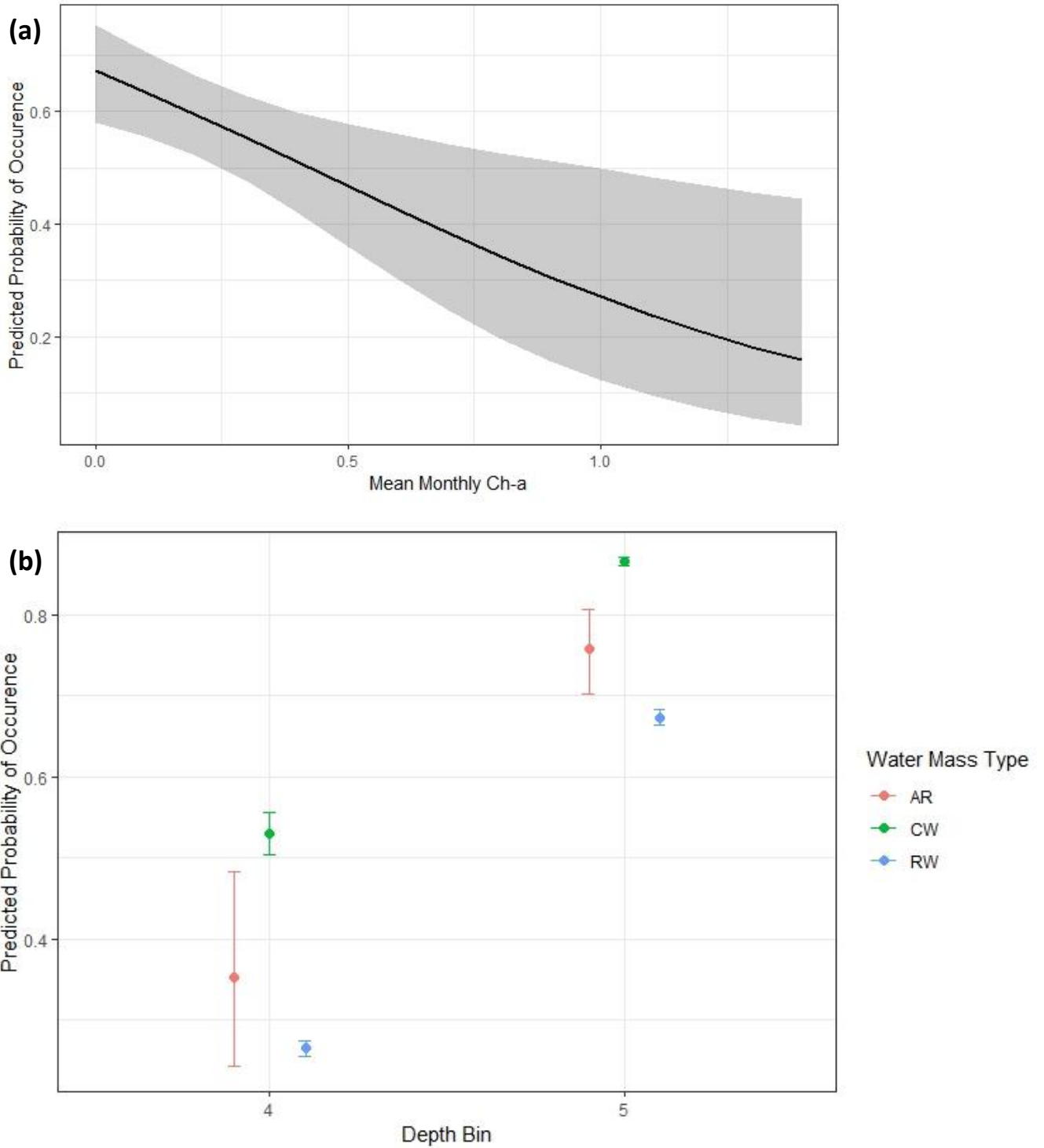Figure 12. Predicted probability of *Sigmops elongatus* occurrence during day (a) and night (b) in relation to mean monthly Chl-a (a), depth bin (b), and water mass type (b).

3.2.3.3 *Sigmops elongatus* Biomass: Data Selection

For both day and night *S. elongatus* mean biomass models all water masses except for MIX (AR, CW, and RW) were included in the full models along with both continuous environmental variables (monthly Chl-*a* and distance to 200-m isobath; Table 5). In the full day mean biomass model for *S. elongatus* only data collected from 200 – 600 m and 600 – 1000 m were included in the full model and in the full night mean biomass model only data collected from 0 – 200 m and 200 – 600 m were included in the full model due to insufficient data in the other depth bins (Table 5).

3.2.3.4 *Sigmops elongatus* Biomass: Minimum Adequate Model (MAM) Results

Predicted mean *S. elongatus* biomass was best explained by the interaction between depth bin and water mass during both day and night (Figure 13, Table 6 and 7). During the day mean predicted *S. elongatus* biomass was highest in the 600 - 1000 m depth bin (Figure 13). The water mass with the highest predicted *S. elongatus* biomass was AR (0.28 g 10^4 m^{-3}), followed by RW (0.17 g 10^4 m^{-3}), and then CW (0.10 g 10^4 m^{-3}; Figure 13). AR and RW had significantly greater predicted mean *S. elongatus* biomass than CW, but they were not significantly different from each other (Figure 13). In the 200 - 600 m depth bin predicted *S. elongatus* biomass was significantly higher within RW (0.05 g 10^4 m^{-3}; Figure 13) than AR and CW which shared the same predicted mean biomass value (0.002 g 10^4 m^{-3}; Figure 13).

At night all water masses reached highs in *S. elongatus* predicted mean biomass in the 200 - 600 m depth bin and lows in mean biomass in the 0 - 200 m depth bin (Figure 13). In the 200 - 600 m depth bin *S. elongatus* predicted mean biomass was significantly higher in RW (0.31 g 10^4 m^{-3}) than AR (0.14 g 10^4 m^{-3}) and CW (0.10 g 10^4 m^{-3}; Figure 13). Within the 0 - 200 m depth bin predicted mean *S. elongatus* biomass was also significantly higher in RW (0.15 g 10^4 m^{-3}) than AR (0.01 g 10^4 m^{-3}) and CW (0.05 g 10^4 m^{-3}; Figure 13). The main difference between water masses came between AR and CW with CW having significantly higher predicted *S. elongatus* biomass in the 0 - 200 m depth bin than AR (0.05 g 10^4 m^{-3} vs 0.01 g 10^4 m^{-3}).
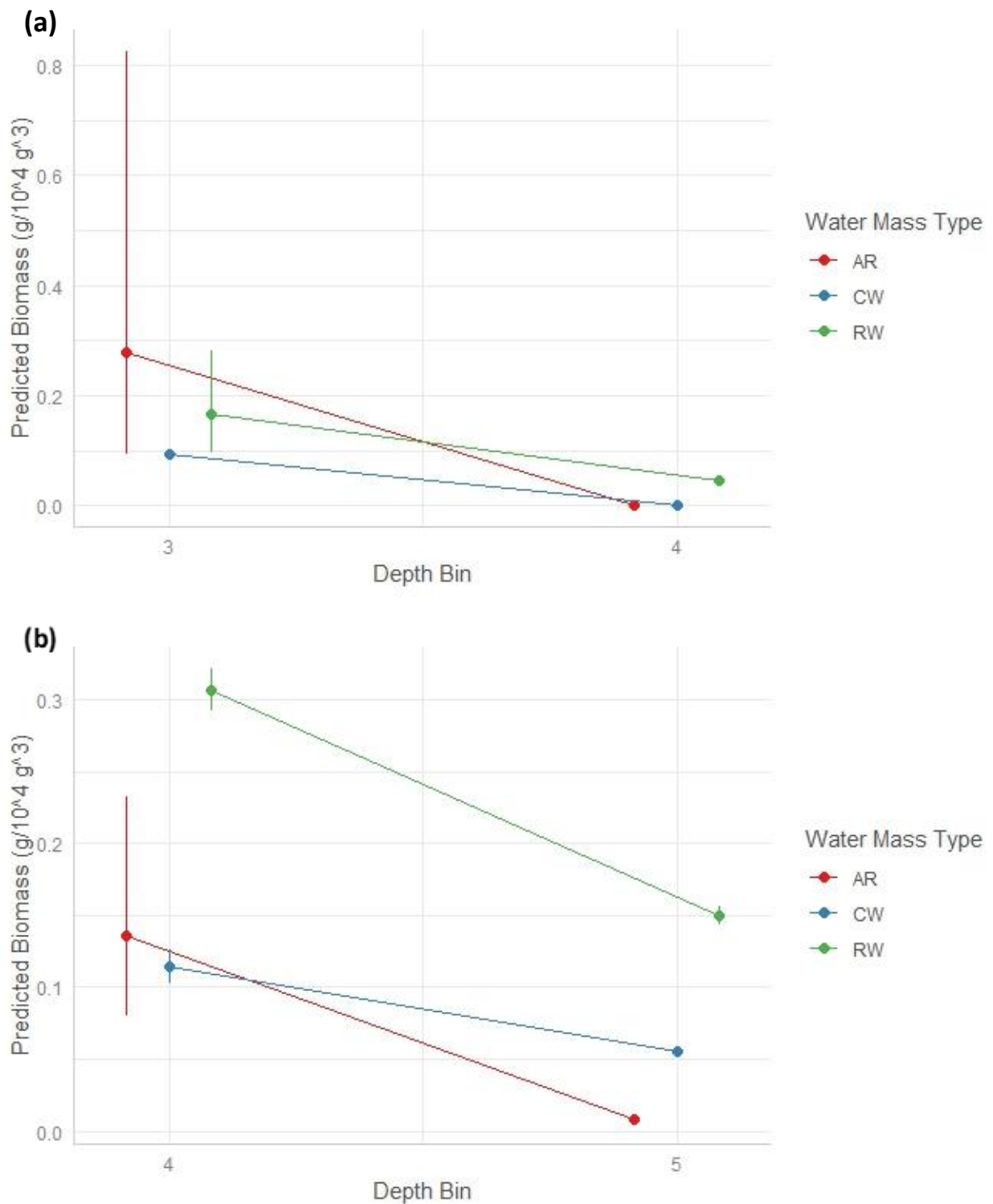
Figure 13. Interaction plot describing the relationship between depth bin and water mass type for predicted mean biomass values of *Sigmops elongatus* during day (a) and night (b).

3.2.4. *Chauliodus sloani*

3.2.4.1 *Chauliodus sloani* Presence-Absence: Data Selection

For both day and night *C. sloani* presence-absence models all water masses except for MIX (AR, CW, and RW) were included in the full models along with both continuous environmental variables (monthly Chl-*a* and distance to 200-m isobath; Table 5). In the full daytime presence-absence model for *C. sloani* only data collected from 200 - 600 m were included in the full model due to insufficient data in the other depth bins (Table 5). For this reason, the random effect term (deployment) was dropped from the full daytime model. The full night presence-absence model for *C. sloani* excluded trawl samples from the 600 - 1000 m, 1000 - 1200 m, and 1200 - 1500 m depth bins due to insufficient data (Table 5).

3.2.4.2 *Chauliodus sloani* Presence-Absence: Minimum Adequate Model (MAM) Results

The probability of *C. sloani* occurrence during the day was not significantly affected by any of the variables (Table 6).

The probability of *C. sloani* occurrence at night was best explained by the interaction between depth bin and water mass (Figure 14, Table 7). The predicted probability of *C. sloani* occurrence within AR and RW was highest within the 200 – 600 m depth bin (AR: 47%, RW: 82%) and lowest within the 0 - 200 m depth bin (AR: 34%, RW: 46%; Figure 14). The predicted probability of *C. sloani* in CW was the opposite of AR and RW with the highest predicted probability coming within the 0 - 200 m depth bin (58%) and the lowest coming within the 200 - 600 m depth bin (46%; Figure 14). The differences between water masses were largely insignificant except in the 200 – 600 m depth bin where predicted *C. sloani* occurrences in RW were significantly higher than CW and AR (Figure 14).

The probability of *C. sloani* occurrence at night was also best explained by the distance to the nearest 200-m isobath (Figure 14, Table 7). The predicted probability of *C. sloani* occurrence decreased linearly with increasing distance from the shelf break with the nearest stations having predicted probabilities of *C. sloani* occurrence of 76% while the farthest stations from the shelf break had predicted probabilities of occurrence of 33% (Figure 14).
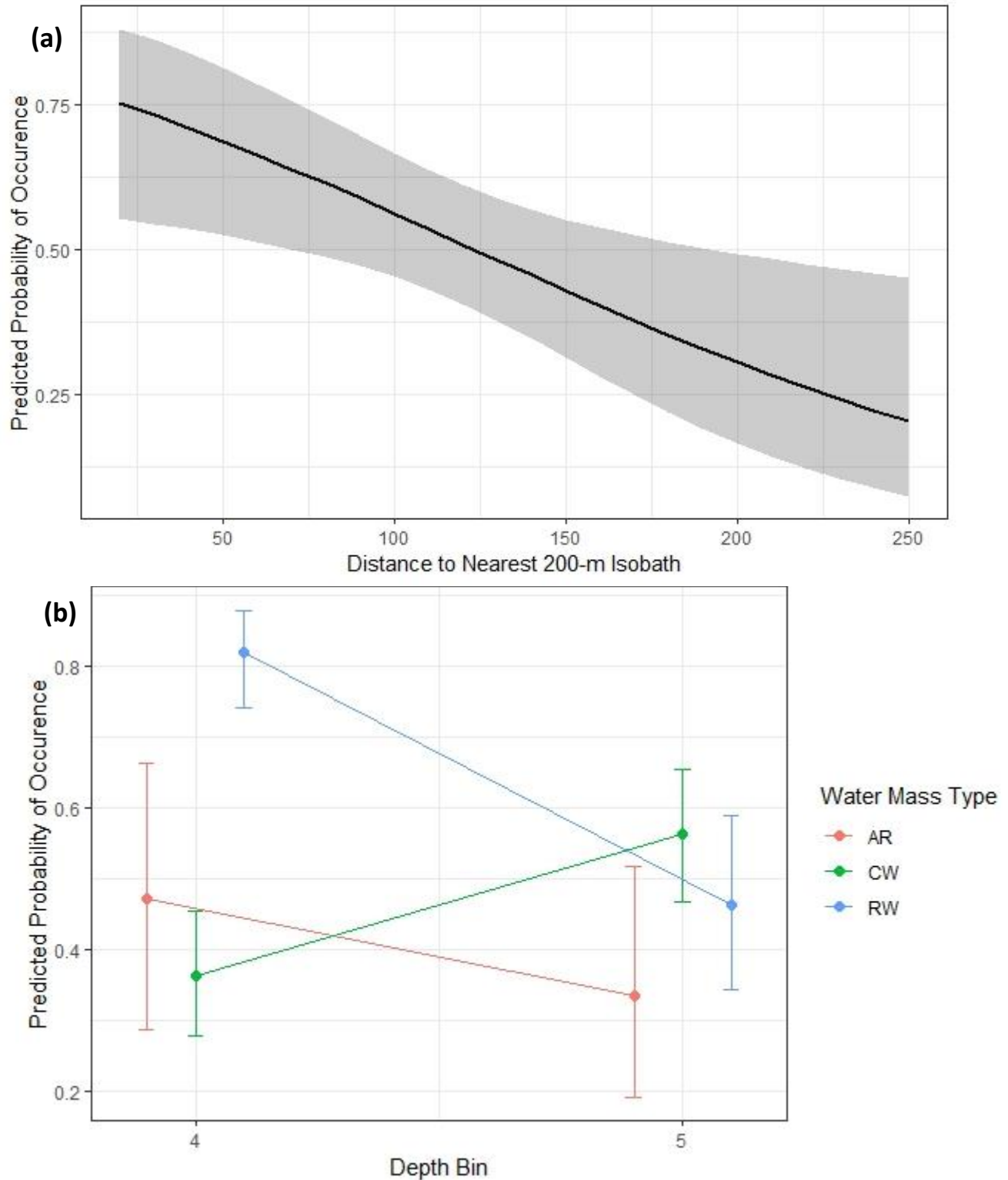
Figure 14. Interaction plot describing the relationship between depth bin and water mass type for predicted probability of occurrence values of *Chauliodus sloani* at night (a). Predicted probability of *Chauliodus sloani* occurrence in relation to distance to 200-m isobath at night (b).

3.2.4.3 *Chauliodus sloani* Biomass: Data Selection

For both day and night *C. sloani* mean biomass models all water masses except for MIX (AR, CW, and RW) were included in the full models along with both continuous environmental variables (monthly Chl-*a* and distance to 200-m isobath; Table 5). In the full daytime mean biomass model for *C. sloani* only data collected from 200 – 600 m were included in the full model due to insufficient data in the other depth bins (Table 5). For this reason, the random effect term (deployment) was dropped from the full daytime model. The full night mean biomass model for *C. sloani* only included trawl samples from the 0 - 200 m and 200 - 600 m depth bins due to insufficient data in the other depth bins (Table 5).

3.2.4.4 *Chauliodus sloani* Biomass: Minimum Adequate Model (MAM) Results

Mean *C. sloani* biomass during the day was best explained by mean monthly Chl-*a* (Figure 9, Table 6). The relationship between predicted mean *C. sloani* biomass and monthly Chl-*a* was generally cubic with peaks in predicted biomass of 0.09 g 10^4 m^{-3} at 0.42 mg m^{-3} and another peak of 0.06 g 10^4 m^{-3} at 1.38 mg m^{-3} (Figure 15). Predicted *C. sloani* mean biomass reached lows of 0.01 g 10^4 m^{-3} at 0.1 mg m^{-3} and 1.10 mg m^{-3} (Figure 15).

Mean *C. sloani* biomass at night was best explained by depth bin and water mass type (Figure 15, Table 7). Predicted mean *C. sloani* biomass was highest within the 200 – 600 m depth bin (0.17 g/10^4 m^3) and lowest within the 0 – 200 m depth bin (0.11 g/10^4 m^3; Figure 9). Predicted mean *C. sloani* was highest within RW (0.25 g/10^4 m^3), followed by CW (0.11 g/10^4 m^3), and last by AR (0.05 g/10^4 m^3; Figure 15). The differences between depth bins and water mass types were insignificant as their prediction intervals significantly overlapped (Figure 15). There was additionally significant variability in *C. sloani* predicted biomass between deployments (random effect) which may potentially indicate an additional driver of *C. sloani* biomass distributions not captured in the model.
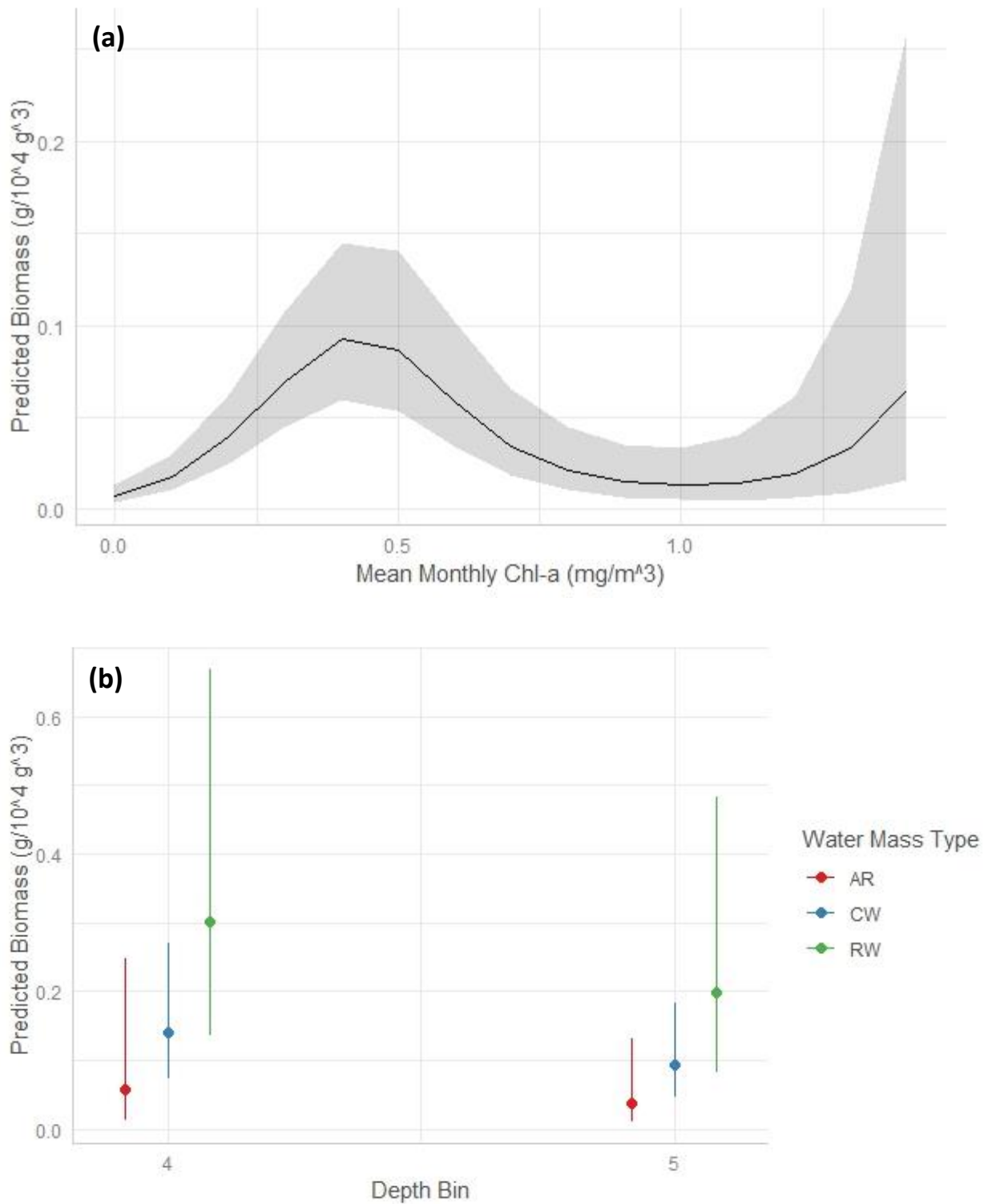
Figure 15. Predicted mean *Chauliodus sloani* biomass in relation to mean monthly Chl-a during the day (a), depth bin at night (b), and water mass type at night (b).

3.2.5. *Photostomias guernei*

3.2.5.1 *Photostomias guernei* Presence-Absence: Data Selection

For the full daytime presence-absence model for *P. guernei* all water masses except for MIX (AR, CW, and RW) and data collected from 600 – 1000 m were included in the full model due to insufficient data in MIX and the other depth bins (Table 5). The exclusion of all but a single depth bin meant that deployment (random effect) and the interaction term between depth bin and water mass type were dropped from the full daytime model (Table 5). For the full nighttime presence-absence model for *P. guernei* only data collected from AR and CW and the 200 – 600 m and 600 – 1000 m depth bins were included due to insufficient data in MIX, RW, and the other depth bins (Table 5). Both continuous environmental variables (monthly Chl-*a* and distance to 200-m isobath) were included in both full models (Table 5).

3.2.5.2 *Photostomias guernei* Presence-Absence: Minimum Adequate Model (MAM) Results

The probability of *P. guernei* occurrence during the day was only significantly affected by distance to the nearest 200-m isobath (Figure 16, Table 6). The predicted probability of *P. guernei* occurrence increased with increasing distance from the shelf break with the nearest station having a predicted probability of occurrence of 30% and the furthest station having a predicted probability of occurrence of 55% (Figure 16).

The probability of *P. guernei* occurrence at night was only significantly affected by depth bin (Figure 16, Table 7). The predicted probability of *P. guernei* occurrence was highest in the 200 – 600 m depth bin (28%) and lowest in the 600 – 1000 m depth bin (12%) but these differences were determined to be insignificant due to the overlap in their prediction intervals (Figure 16).
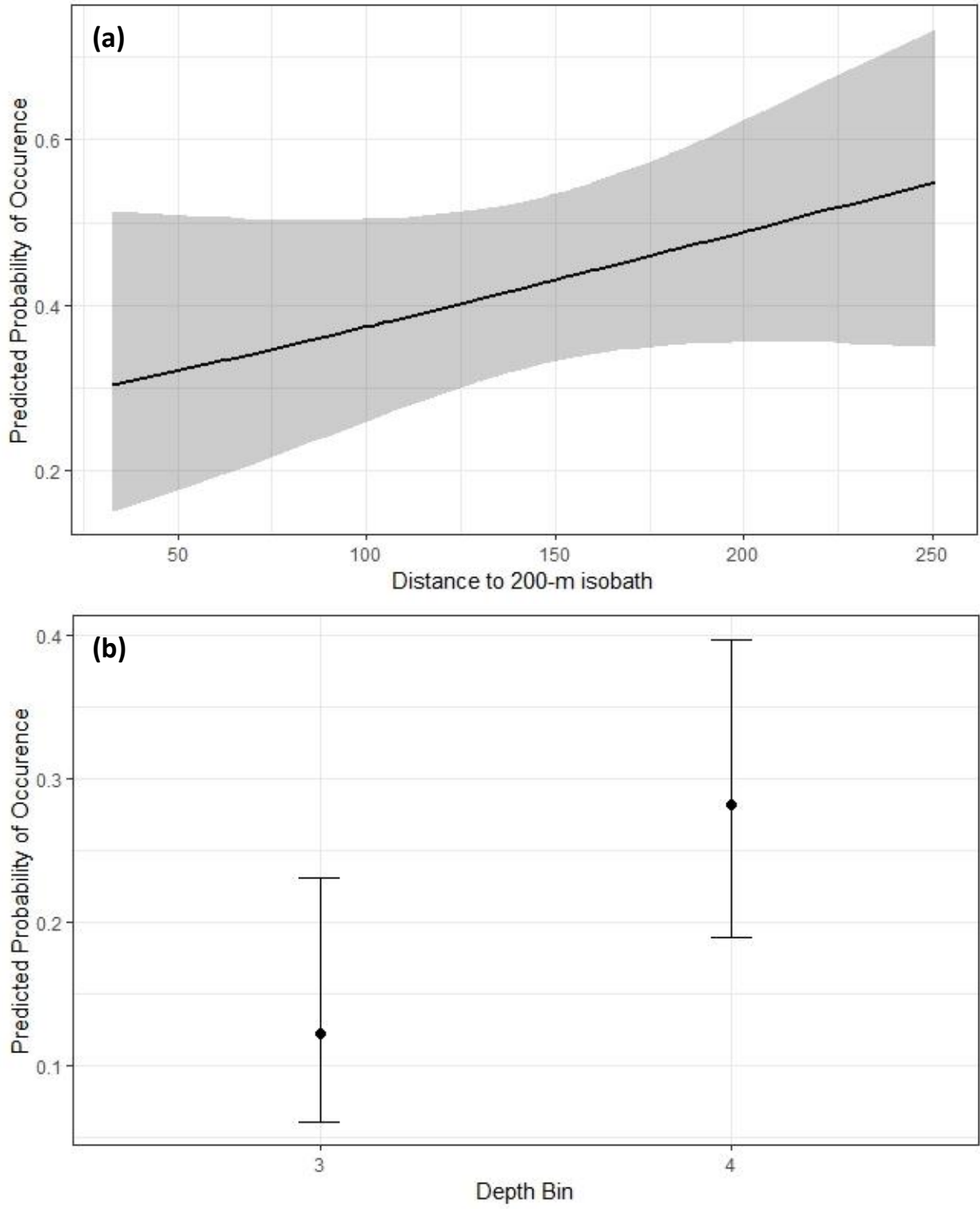
Figure 16. Predicted probability of *Photostomias guernei* occurrence in relation to distance to the nearest 200-m isobath during the day (a) and depth bin at night (b).

3.2.5.3 *Photostomias guernei* Biomass: Data Selection

For the full daytime mean biomass model for *P. guernei* all water masses except for MIX (AR, CW, and RW) and data collected from 600 - 1000 m were included in the full model due to insufficient data in MIX and the other depth bins (Table 5). The exclusion of all but a single depth stratum meant that deployment (random effect) and the interaction term between depth bin and water mass type were dropped from the full daytime model (Table 5). For the full nighttime mean biomass model for *P. guernei* only data collected from AR and CW and the 200 – 600 m and 600 – 1000 m depth bins were included due to insufficient data in MIX, RW, and the other depth bins (Table 5). Both continuous environmental variables (monthly Chl-*a* and distance to 200-m isobath) were included in both full day and night mean biomass models (Table 5).

3.2.5.4 *Photostomias guernei* Biomass: Minimum Adequate Model (MAM) Results

Mean *P. guernei* biomass during the day was best explained by distance to the nearest 200-m isobath (Figure 17, Table 6). Predicted mean *P. guernei* biomass decreased with increasing distance from the shelf break with predicted biomass nearest to the shelf break being 0.11 g 10^4 m^{-3} and predicted biomass farthest from the shelf break being 0.04 g 10^4 m^{-3} (Figure 17).

Mean *P. guernei* biomass at night was not sufficiently explained by any of the explanatory variables (Table 7).
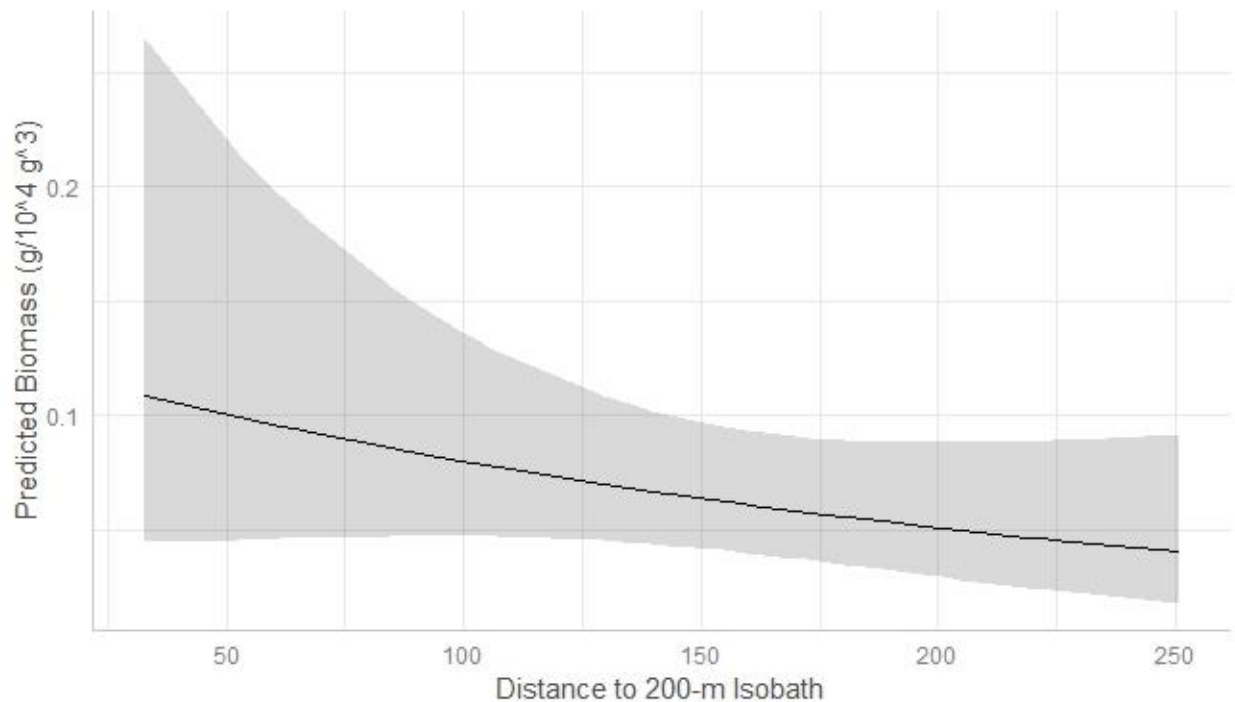
Figure 17. Predicted mean *Photostomias guernei* biomass in relation to distance to the nearest 200 m isobath during the day.

3.2.6. *Stomias affinis*

3.2.6.1 *Stomias affinis* Presence-Absence: Data Selection

For the full daytime presence-absence model for *S. affinis* only data collected from CW and the 200 – 600 m and 600 – 1000 m depth bins were included in the full model due to insufficient data in the other water masses and depth bins (Table 5). The exclusion of all but a single water mass meant that the interaction term between depth bin and water mass type was dropped from the full daytime model (Table 5). For the full nighttime presence-absence model for *S. affinis* only data collected from AR, CW and the 0 - 200 m depth bin were included due to insufficient data in MIX, RW, and the other depth bins (Table 5). The exclusion of all but a single depth stratum meant that deployment (random effect) and the interaction term between depth bin and water mass type were dropped from the full daytime model (Table 5). Both continuous environmental variables (monthly Chl-*a* and distance to 200-m isobath) were included in both full models (Table 5).

3.2.6.2 *Stomias affinis* Presence-Absence: Minimum Adequate Model (MAM) Results

The probability of *S. affinis* occurrence during the day and at night was significantly affected by distance to the nearest 200-m isobath (Figure 18 and 19, Table 6 and 7). During both day and night, the predicted probability of *S. affinis* occurrence increased with increasing distance from the shelf break (Figure 18 and 19). During the day the predicted probability of *S. affinis* occurrence at the station closest to the shelf break was 34% and the predicted probability at the furthest station from the shelf break was 64% (Figure 18). At night the predicted probability of *S. affinis* occurrence at the closest station to the shelf break was 5% and the predicted probability at the station furthest from the shelf break was 67% (Figure 19).

The probability of *S. affinis* occurrence during the day was also significantly affected by monthly Chl-*a* (Figure 18, Table 6). The predicted probability of *S. affinis* occurrences generally increased with increasing monthly Chl-*a* values with the predicted probability of *S. affinis* occurrence increasing 11% from the lowest monthly Chl-*a* station (17%) to the station with the highest mean monthly Chl-*a* value (28%, Figure 18). There was a large increase in predicted occurrences from 0.17 mg m^{-3} to 0.50 mg m^{-3} where the predicted probability of *S. affinis* occurrence increased from 17% to 70% before decreasing back to 20% at 1.00 mg m^{-3} (Figure 18).
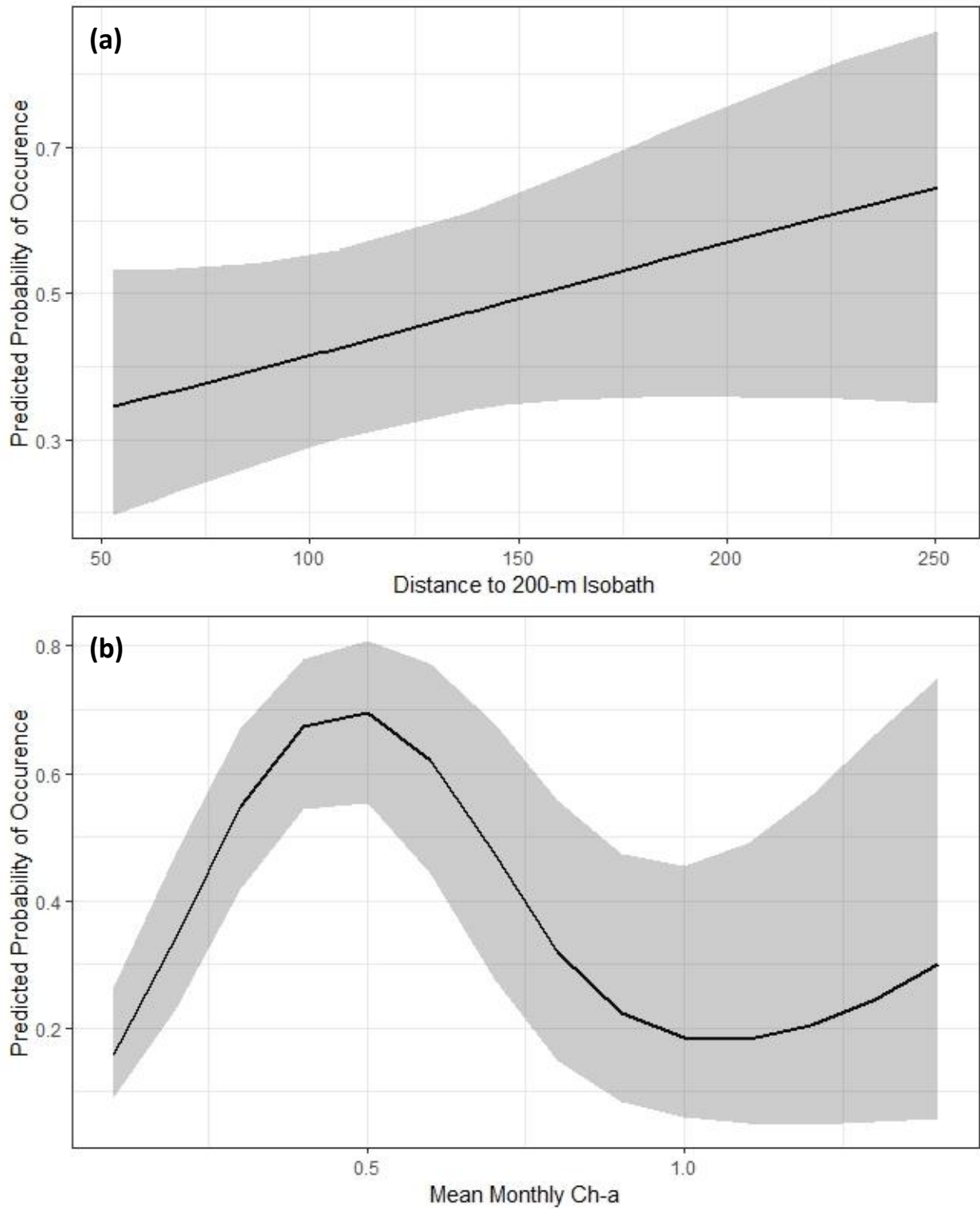
Figure 18. Predicted probability of *Stomias affinis* occurrence during the day in relation to distance to the nearest 200-m isobath (a) and mean monthly Chl-a (b).
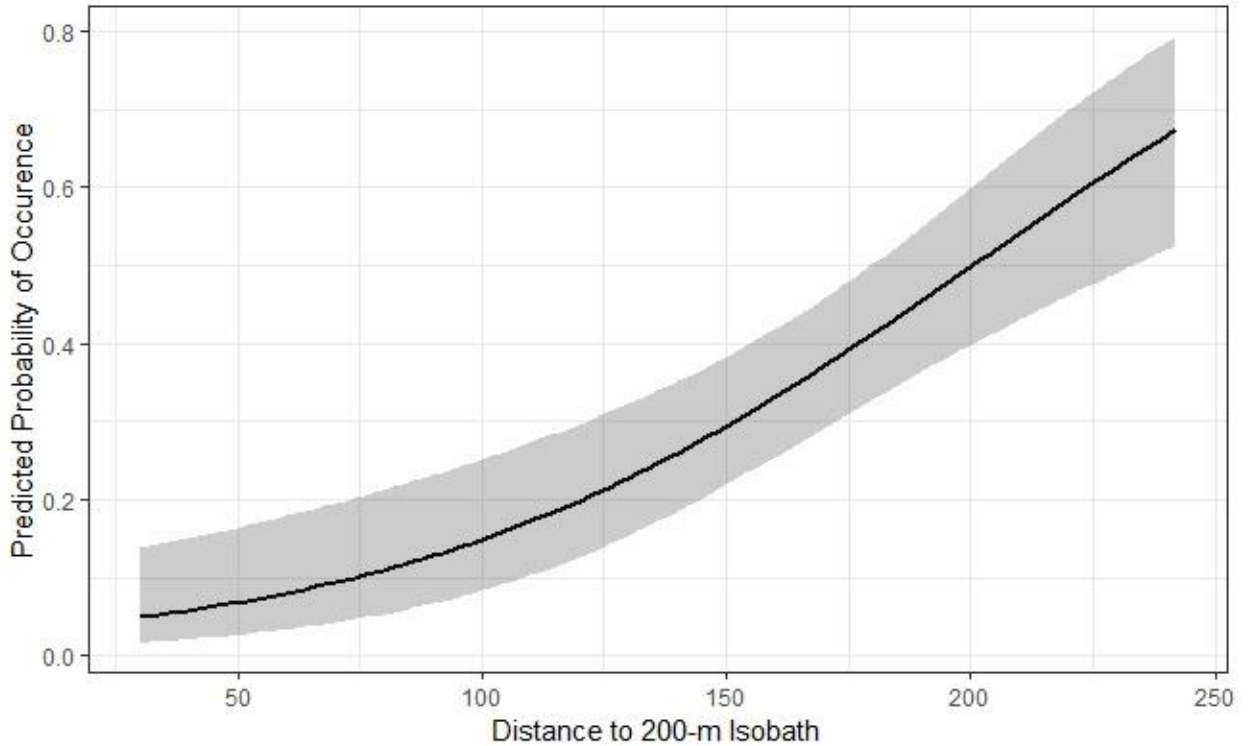
Figure 19. Predicted probability of *Stomias affinis* occurrence at night in relation to distance to the nearest 200 m isobath.

3.2.6.3 *Stomias affinis* Biomass: Data Selection

For the full daytime mean biomass model for *S. affinis* only data collected from CW and the 200 – 600 m and 600 – 1000 m depth bins were included in the full model due to insufficient data in the other water masses and depth bins (Table 5). The exclusion of all but a single water mass meant that the interaction term between depth bin and water mass type was also dropped from the full daytime model (Table 5). For the full nighttime mean biomass model for *S. affinis* only data collected from AR, CW and the 0 – 200 m depth bin were included due to insufficient data in MIX, RW, and the other depth bins (Table 5). The exclusion of all but a single depth bin meant that deployment (random effect) and the interaction term between depth bin and water mass type were also dropped from the full daytime model (Table 5). Both continuous environmental variables (monthly Chl-*a* and distance to 200-m isobath) were included in both full models (Table 5).

3.2.6.4 *Stomias affinis* Biomass: Minimum Adequate Model (MAM) Results

Mean *S. affinis* biomass during the day was best explained by depth bin (Figure 20, Table 6). Predicted *S. affinis* mean biomass during the day was significantly higher within the 600 - 1000 m depth bin (0.20 g 10^4 m^{-3}) than the 200 - 600 m depth bin (0.01 g 10^4 m^{-3}; Figure 20).

Mean *S. affinis* biomass at night was not explained by any of the environmental variables (Table 7).

Figure 20. Predicted mean *Stomias affinis* biomass during the day in relation to depth bin.

4. Discussion

This study calculated the LWRs and examined the spatial distributions of six stomiiform fishes in the northern GoM in relation to various mesoscale oceanographic features such as the LC, LCEs, and the Mississippi River plume. Overall, the LWRs calculated for the stomiiform fishes examined displayed high coefficient of determination values ($R^2 > 0.90$) and five of the six species possessed allometric growth coefficients within the normal range (2.5 – 3.5). In terms of spatial distributions, the main results of this study showed that the stomiiform fishes examined largely display species-specific responses to mesoscale oceanographic features at the temporal and spatial scales examined. The most widespread and consistent trend across taxa was a deepening of vertical distributions in response to the LC and LCEs. The horizontal distributions of the stomiiform fishes were marginally affected by the environmental variables examined with some notable exceptions, namely in response to distance to nearest 200-m isobath (*P. guernei*) and Chl-*a* (*S. elongatus*). In general, this study confirms previous findings that the mesopelagic assemblage in the northern GoM is primarily structured by depth and is only weakly horizontally structured in response to the examined mesoscale oceanographic features. Additionally, this study indicates that responses to such mesoscale oceanographic features are largely species dependent with individual species displaying various responses to the examined features.

4.1. Length-Weight Relationships

The LWRs for six stomiiform fishes in the northern GoM were obtained during this study with all the length-weight models constructed possessing high coefficients of determination values ($R^2 > 0.90$). Of the six species of Stomiiformes analyzed five of the six possessed allometric growth coefficients (parameter *b*) within the 2.5 – 3.5 range highlighted in Froese (2006) as the normal range of allometric growth coefficients in fishes. Of the stomiiform fishes examined three displayed isometric growth (*b* = 3), two negative allometric growth (*b* < 3), and one exhibited positive allometric growth (*b* > 3). While few studies used DWs in their calculations of LWRs when comparisons are made using the obtained LWRs based upon WWs the allometric growth coefficients obtained were in line with previous studies from the western GoM and Tropical Atlantic (Chi-Espínola et al., 2023; Lopez-Perez et al., 2020).

Chauliodus sloani, *P. guernei*, and *S. affinis* all exhibited isometric growth. Isometric growth means that these taxa grew proportionally the same in weight and length as they aged and

indicates that they did not exhibit any significant changes in body form as they grew (Froese 2006). While the allometric growth coefficients of *P. guernei* (2.76 ± 0.45 vs. 2.94) and *S. affinis* (2.93 ± 0.3 vs. 3.07) were not significantly different from the results of Sutton and Hopkins (1996) the allometric coefficient of *C. sloani* (2.85 ± 0.23 vs. 2.54) was significantly higher. Differences in the allometric growth coefficients between studies may be related to seasonality as samples collected in Sutton and Hopkins (1996) were collected year-round while the current study only analyzed samples collected from May to August. Additionally, differences in individual's nutritional condition between studies may have also resulted in the observed differences as smaller individuals in relatively worse nutritional condition than larger individuals can elevate the allometric growth coefficient (Froese 2006).

      Sigmops elongatus and *C. pseudopallida* exhibited negative allometric growth. Negative allometric growth in fishes is typically characteristic of individuals becoming more elongated with age which is typical of the elongated body plans and high-water contents of taxa like *S. elongatus* and *C. pseudopallida* (Lopez-Perez et al., 2020). The growth form of *Sigmops elongatus* agreed with findings by Lancraft et al., (1988) who used a similar methodology in obtaining LWRs (*b* = 2.305 vs. 2.628). While LWR derived from DWs for *C. pseudopallida* was unable to be compared due to a lack of studies using DWs when using its WW derived LWR its allometric growth coefficient was in line with other studies from the region (Chi-Espínola et al., 2023).

      Cyclothone pallida was the lone species that exhibited positive allometric growth (faster growth in weight than length) which is atypical of the genus *Cyclothone,* which usually exhibits negative allometric growth (Lopez-Perez et al., 2020; Chi-Espínola et al., 2023). Direct comparisons to other studies using the LWRs derived from DWs were not possible due to a lack of studies that used a similar methodology. When the LWR of *C. pallida* was calculated using WWs it was considered to have isometric growth, which was similar to the WW derived estimate of *C. pseudopallida*. Lopez-Perez et al. (2020) found that the growth form for an individual species may change depending on whether dry weights or wet weights were used. It appears likely that this is what is occurring with *C. pallida* in this study. It is interesting that *C. pseudopallida* given its similarity to *C. pallida* did not display a similar trend especially considering their allometric growth coefficients derived from WWs were similar (*C. pallida*: 2.7359 vs. *C. pseudopallida*: 2.9331). However, *C. pallida* and *C. pseudopallida* do have different water and lipid contents

which could potentially contribute to these differences in DW derived LWR estimates (M. Kayama and Y. Ikeda, 1975).

The allometric growth coefficient obtained for *S. elongatus* fell outside the normally accepted range (b = 2.5 – 3.5). While allometric growth coefficients outside the normal range are often derived from limited size ranges, the size range used (1.25 - 12.05 cm) was similar to the size classes used in Lancraft et al. 1988 (2.0 – 15.0 cm). A potential reason for the relatively small allometric growth coefficient obtained for *S. elongatus* is a difference in the relative nutritional condition of "small" and "large" individuals. Small individuals that are in a better nutritional condition at the time of sampling compared to larger individuals have the tendency to shift the allometric growth coefficient downward (closer to two; Froese 2006). Given that the *S. elongatus* specimens used in the calculation of its LWR came from multiple cruises and the relative conditions of individual specimens was not investigated it is difficult to determine an exact cause for the potential differences in nutritional condition. Ultimately it may simply be due to the variability surrounding calculating LWRs.

Calculations of LWRs in general can be highly variable with size range, nutritional condition, gonadal mass, season, gut content, and preservation type all potentially influencing the calculated parameters (Froese, 2006; Lopez-Perez et al., 2020; Mazumder et al. 2016). Given that all the individuals used in the estimations of the examined taxa's LWRs were collected from May to August the inclusion of individuals from different seasons may be beneficial. Future studies may also consider the use of eviscerated dry weights as recommended in Lopez-Perez et al. (2020) due to its ability to limit the effects of gonadal mass and gut content on the obtained parameters. Additionally, the inclusion of larger size classes and the use of multiple weight types to calculate LWRs is recommended especially in comparison to other studies that often use larger size classes and different methodologies in LWR calculations. Growth stanzas, which were not considered in the present study, could be potentially investigated considering that they have been noted in stomiiform fishes in other studies of LWRs (e.g., Czudaj et al., 2022). The LWRs presented in the current study add to the existing but limited literature on LWRs in mesopelagic fishes and provide useful LW parameters for the conversion of lengths to either WWs or DWs for the examined taxa.

4.2. Spatial Structuring

4.2.1 Effect of Water Mass on Vertical Distributions

Water masses impact on the vertical distributions of the examined stomiiform fishes was widespread with the interaction between water mass and depth bin being retained in some form within four of the six species analyzed (*C. pallida*, *C. pseudopallida*, *S. elongatus*, and *C. sloani*). While the alterations to vertical distributions were largely species specific there were general patterns seen across taxa, the most prevalent being a deepening of day and night vertical distributions within LC origin waters compared to the other water masses.

One of the primary theories as to why the vertical distributions of mesopelagic fishes are shifted downward within anticyclonic eddies is related to alterations of individuals' light comfort zones (Penna et al. 2021). Light comfort zones (LCZs) refer to an organism's preferred range of irradiance levels which has been hypothesized to optimize one's ability to forage and avoid visual predation (Kaartvedt et al., 2017). Light penetration depth has been pointed to as a first order driver structuring the vertical distributions of mesopelagic organisms with studies on various spatial and temporal scales and in various biogeographical regions throughout the World Ocean supporting this assertion (Aksnes et al., 2017; Kaartvedt et al. 2017; Langbehn et al. 2019; Widder and Frank, 2002). While studies of mesoscale eddies' effect on the vertical distributions of mesopelagic organisms and light intensity together are rare (but see: Penna et al., 2021) given that the depth of the DSL is known to fluctuate based on relatively small changes in light (e.g., by weather, lunar cycle, etc.) it is reasonable to assume that the large scale alteration of optical properties within the water column caused by the LC and LCEs would alter the vertical distributions of mesopelagic organisms in some way (Kaartvedt et al., 2017; Last et al., 2016; Strömberg et al. 2002; Tarling et al. 1999).

The LC and LCEs are associated with deeper light penetration than background Gulf waters (due to lower productivity) and thus could shift LCZs downwards which may explain the downward shifts seen in *C. pallida*, *C. pseudopallida*, *S. elongatus*, and *C. sloani* (Zhang et al., 2023). Alterations to LCZs may also explain the limited magnitude of DVM and/or the reduced DVM rates seen in *S. elongatus* and *C. sloani* under LC conditions. While alterations to light penetration depth is usually discussed in the context of daytime vertical distributions, light penetration has also been known to affect nighttime distributions as well (Drazen et al., 2011; Last

et al., 2016). Under LC conditions diel vertically migrating organisms' upper depth range may be deeper compared to Gulf Common water, thus altering the magnitude of their migration.

The effects of RW on the vertical distribution of *C. pallida* may offer additional support for light penetration depth being the primary driver of changes in vertical distributions seen in the current study. There was a notable upward shift in the vertical distribution of *C. pallida* within RW which may be due to an upward shift in LCZ of *C. pallida*. RW is characterized by high productivity and high turbidity (opposite of LC and LCEs) which will theoretically lead to shallower light penetration. Under the influence of RW organism's LCZs may be shifted upwards and thus explain the upward shift seen in the vertical distribution of *C. pallida*. Additionally, an increased probability of occurrence within the upper mesopelagic (200 - 600 m) within RW was observed in *C. sloani*. This could potentially be interpreted as a decrease in the DVM rates of *C. sloani* within RW potentially because of low salinity conditions (Luo et al., 2000). However, the predicted occurrence of *C. sloani* was not significantly different from the other water masses within the epipelagic and the low salinity plume is contained to the upper 15 -30 m of the water column. This may indicate that the change in predicted probabilities may be due to an upward shift in individuals from the lower mesopelagic (600 – 1000 m). Adding support to this hypothesis is the fact that the 600 – 1000 m depth bin for *C. sloani* at night was not analyzed in the current study due to only a single specimen being present in RW in that depth bin, which was lowest among the water masses analyzed. This potentially indicates that *C. sloani* is exhibiting a shallower distribution within RW than the other water masses.

Another proposed hypothesis behind the deepened vertical distributions and alterations of DVM patterns seen in anticyclonic eddies is related to downwelling conditions (Boswell et al., 2020; Della Penna & Gaube, 2020; Godo et al., 2012). The center of anticyclonic eddies is characterized by downwelling conditions and thus it has been suggested that the deepening of the DSL is related to either the passive transport of lethargic mesopelagic organisms and/or mesopelagic organisms actively following their prey that have been shifted downward (Godo et al., 2012). DVM behavior has also been hypothesized to be altered by LC conditions due to the increased metabolic cost of migrating within LC conditions due to downwelling but also the potential increased distance if the organism's daytime distribution is shifted downwards (Boswell et al., 2020).

Aside from alterations to LCZs and downwelling conditions, another potential factor in the deeper vertical distributions seen within LC conditions is thermal constraints. While unlikely in *C. pallida* and *C. pseudopallida* due to their persistence throughout the water column, it could be a factor for the larger stomiiform fishes examined due to their relatively narrower vertical ranges. Thermal constraints to vertical distributions have been hypothesized in *C. sloani* in the tropical Atlantic where the population forgoes DVM and resides permanently at depth (~800 m) primarily below 12 – 15 ℃ (Eduardo et al. 2020). Unlike the tropical Atlantic however, the *C. sloani* population in the northern GoM is still present in some degree in the epipelagic zone of the LC despite the temperatures being higher than 12 – 15 ℃, so temperature is not entirely sufficient in explaining changes to vertical distributions in this case but could be investigated further.

Disentangling the relative roles that light penetration depth, downwelling conditions, and temperature play in the observed patterns is not possible in the current study because they covary within the GoM setting. However, given that light penetration is already a likely first-order driver of the vertical distributions of mesopelagic organisms and potentially explains all the observed patterns it seems likely that it is the primary driver of the observed alterations in vertical distributions, especially given that the role of mesopelagic organisms as passive particles in water column is disputed and the prey sources of many of the mesopelagic taxa examined are also largely structured by light (Kaartvedt et al., 2009; Kaartvedt et al., 2023). Additionally, the effects of downwelling and/or temperature would not explain the upward shifts in vertical distributions seen in *C. pallida* and potentially *C. sloani*. Ultimately *in situ* light measurements are required to demonstrate that alterations of LCZs are driving the observed vertical patterns.

Stomias affinis and *P. guernei* were not observed to be vertically structured by water mass in the present study. The LCZs of mesopelagic organisms can potentially cover a large range of light levels (up to 10 orders of magnitude) so the changes in light penetration depth may have not been substantial enough to affect the preferred LCZs of *S. affinis* or *P. guernei* (Kaartvedt et al., 2017). Additionally, *S. affinis* and *P. guernei* are highly mobile taxa so they may be unaffected by downwelling conditions if that is the primary driver of vertical distributions.

4.2.2. Note on MIX Water Mass Type (Vertical Distributions)

Conclusions about the MIX water mass type's impact on the vertical distribution of the examined taxa are largely inclusive due in part to the low relative number of MIX stations sampled

and the high variability at these stations. As a result, it was only able to be investigated in *C. pallida* and *C. pseudopallida*. In terms of vertical distributions, *C. pallida* and *C. pseudopallida* distributions within MIX were either indistinguishable from their distributions in AR, CW, and RW or they tended to fall in between AR and CW. This seems to indicate that the vertical distributions of the examined *Cyclothone* were deepened in some cases within MIX but not in the same magnitude as AR. This potentially supports the conclusions of Johnson et al. (2019) that proposed MIX as an "intermediate" between AR and CW in terms of structuring the mesopelagic assemblage. However, as mentioned previously due to the high variability in biomass and in predicted occurrence within MIX it is difficult to draw definitive conclusions about MIX's impact on the mesopelagic assemblage.

The MIX water mass was notably not representing a single set of physical conditions as processes at the LC boundary likely occurred at finer scales than could be simulated in the classification process (i.e., < 3 h and $< 4 \times 4$ km; Johnson et al., 2019). As a result, a variety of oceanographic conditions (e.g., convergent or divergent fronts) may be taking place within MIX that are simply not represented in the study and may have resulted in the high variability in mesopelagic biomass observed. Boundary regions are highly dynamic and thus their impacts on the mesopelagic assemblage may be difficult to discern, especially at the scales examined. Further sampling of these regions and potentially further fine scale designations of their oceanographic conditions may help to clarify their potential impacts on the mesopelagic assemblage in future studies.

4.2.3. Reponses to Coastal Influences (Distance to 200-m Isobath) and Productivity (Mean Monthly Chl-a)

There was evidence of limited horizontal structuring in response to distance to nearest 200-m isobath, with *P. guernei* and *S. affinis* having increased probabilities of occurrence with greater distance from the shelf break and *C. sloani* having increased probabilities closer to the shelf break. This potentially indicates horizontal structuring in response to coastal influences as has been previously noted in tuna and billfish larvae which partition their habitats with certain species preferring coastal or oceanic conditions (Pruzinsky et al., 2020; Rooker et al., 2012).

The increased probability of capture of *C. sloani* closer to the shelf break aligns with previous literature that has noted its occurrence along continental slopes and in coastal regions in

areas such as North Carolina, Australia, the Western GoM and the Arbian Sea (Aguilar-Medrano et al., 2020; Butler et al., 2001; Gartner et al., 2008; Williams et al., 2001). Nearshore regions in northern GoM are characterized by high terrestrial runoff and high Chl-*a* and thus are likely to support greater primary and secondary productivity which *C. sloani* may be taking advantage of.

In previous studies *P. guernei* and *S. affinis* have been found in slope and offshore regions though literature on their horizontal distributions is rather limited (Aguilar-Medrano et al., 2020; Butler et al., 2001). In the present study the increased probabilities of *P. guernei* and *S. affinis* capture further from the shelf break may indicate that they are primarily oceanic species in the northern GoM perhaps in response to presumed limited vertical ranges offered in nearshore waters. Interestingly, *P. guernei* displayed decreased biomass further away from the shelf break at night (the inverse of its predicted occurrence) which potentially indicates an increase in smaller (potentially juvenile) *P. guernei* further from the shelf break. As previously discussed, other pelagic larval fishes (e.g., Swordfish and Tuna) often utilize these offshore oligotrophic regions so these areas may offer a favorable habitat for smaller *P. guernei* (Pruzinsky et al., 2020; Rooker et al., 2012).

In terms of productivity, the examined taxa largely displayed no evidence of structuring in response to mean monthly Chl-*a*. On the global scale mesopelagic fish biomass is largely correlated with upper ocean productivity (Proud et al. 2017). However, on smaller spatial and temporal scales (e.g., 10 – 100 kms, days – months) the connection between mesopelagic fish biomass and productivity is not always apparent and can often be complex (Saijo et al., 2017, Woods et al. 2023). The lack of structuring observed in response to Chl-*a* may be due to spatial and temporal lags between primary productivity and mesopelagic fish biomass and occurrence which were not accounted for in the present study but should be considered in the future. Overall, this study suggests that bottom-up processes are not significantly impacting the examined stomiiform fishes' distribution patterns at the scales examined which suggests that another potential driver is responsible for the observed patterns.

Sigmops elongatus was an exception to the overall trend with its daytime probability of occurrence inversely related to mean monthly Chl-*a* and RW. Other studies have noted inverse relationships between Chl-*a* and species occurrence specifically in the case of *Electrona antarctica*

in the Southern Ocean (Loots et al., 2007). In *E. antarctica* the inverse relationship with Chl-*a* was due to its decreased abundance north of the Antarctic Polar Front (which represented its northern limit) and its absence in shelf regions (Loots et al., 2007). *Sigmops elongatus* was not significantly affected by distance to 200 m isobath which suggests that its response to Chl-*a* is not related to its pelagic nature and thus may be related to another factor. Predicted mean *Sigmops elongatus* biomass was elevated within RW which suggests that the reductions in occurrence are likely driven by smaller *S. elongatus.* If smaller *S. elongatus* are driving the trend, then potentially they are subjected to greater predation risk within these highly productive areas leading to either greater mortality or avoidance. With fewer "smaller" *S. elongatus* the *S. elongatus* captured would likely be larger individuals which would elevate its predicted mean biomass in these regions. Larger *S. elongatus* are also known to reside deeper in the water column than smaller individuals so they may be largely unaffected by RW or localized areas of high productivity which considering that Chl-*a* was not retained in the biomass model appears to be the case (Lancraft et al. 1988).

There were two cases where Chl-*a* was retained (*C. sloani* and *S. affinis*) and the responses were complex with biomass peaks at around 0.50 mg/m^3. In the case of *S. affinis* the peak in biomass was associated with the station "B175" (Figure 5) which when removed from the model meant that Chl-*a* was no longer retained. Station B175 is in the vicinity of DeSoto Canyon which has the potential to alter the distribution patterns of mesopelagic fishes, as has been the case in other undersea canyons (e.g., Kenchington et al., 2020). Undersea canyons allow deep-living taxa access to the more productive continental slope and can potentially host greater fish diversity, abundance, and biomass which can make them hotspots for upper trophic level taxa (Genin, 2004). However, despite B175 being one of the most sampled stations (sampled during all seven cruises) further work needs to be done in the region to draw any significant conclusions about DeSoto Canyon's potential impacts on the mesopelagic assemblage. A peak in *C. sloani* biomass was also found at station B175 but even when data from station B175 was excluded from analysis the peak remained, likely indicating another driver influencing their distribution patterns.

Evidence of horizontal structuring in the examined taxa in response to coastal influences was limited at the spatial and temporal scales examined. Even in cases where distance to 200 m isobath or Chl-*a* were retained it was often not conserved between day and night models (except: *S. elongatus* and *S. affinis*) which hints at the magnitude of structuring (if present) being marginal.

The limited horizontal spatial structuring observed namely in response to distance to 200 m isobath may be due to the vast majority of the trawl samples analyzed being seaward of the 1500 m isobath. Thus, the limited spatial structuring observed may simply be the edge of a potential spatial gradient. Overall, the limited evidence of horizontal structuring supports previous literature on the mesopelagic fish assemblage in the GoM which has suggested that the assemblage has only limited horizontal structure in the offshore space (Milligan and Sutton, 2020; Ross et al., 2010; Wang et al., 2021).

4.3. Caveats and Future Considerations

4.3.1. Caveats

Studies of biomass are inherently biased by the inclusion of larger individuals which can effectively "drown out" the effects of smaller individuals. This was especially the case in this study due to the MOCNESS's bias towards the collects of smaller specimens. While this bias was probably minimal in the case of the *Cyclothone* examined due to their small range, it was apparent in the analysis of the larger, higher trophic level stomiiform fishes examined whose size range is much wider (e.g., *S. elongatus*). The low numbers of specimens for many examined taxa meant that a relatively small number of larger specimens were weighted more heavily in the models based on biomass which may partially explain the discrepancies between presence-absence and biomass models seen in *S. elongatus* and *P. guernei*.

The modelled data were often characterized by high variability, which makes detection of patterns in the data more difficult. The high variability seen in the biomass data is likely partially related to the patchy distribution of mesopelagic fishes at fine scales (10s -100s m). Mesopelagic fishes are known to occur in aggregations with other pelagic fauna and have been observed to exhibit patchy distributions patterns that may be largely structured by small scale environmental cues (Auster et al., 1985; Greenlaw et al., 1985; Duhamel et al., 2000). Considering that this study was conducted using trawl data it is difficult to determine how much influence these fine scale cues have on the study's outcomes and how much this "patchiness" is potentially obscuring potential structuring patterns on the spatial and temporal scales utilized.

The high variability seen in the model data is also likely related to the larger stomiiform fishes examined being inherently rare due to their position as higher trophic level predators.

Modeling the spatial distributions of rare species in general is difficult due to methodological restraints and low abundances (Zhang et al., 2020). As a result, the models for a few taxa, namely *P. guernei* and *S. affinis* were largely based on a handful samples (20 – 30) which may have led to high variability in the generated predicted occurrence and biomass values. Additionally, in these cases the interaction between depth bin and water mass was not always investigated due to limited sample sizes particularly in the different water masses (except CW). As a result, many of the observed patterns in vertical distributions seen in other taxa (e.g., *C. pallida* and *C. sloani*) may have been present but simply could not be investigated.

In terms of sampling, less sampling was conducted in the mesoscale features examined (e.g., LC, LCEs, and river plumes) compared to CW which meant that not all water masses could be compared for all taxa (namely MIX). Additionally, the depth bins utilized in sampling were rather broad which may have obscured the impacts on vertical distributions. The use of broad depth bins also made determining the magnitude of the alterations to vertical distributions seen in *C. pallida*, *C. pseudopallida*, *S. elongatus,* and *C. sloani* difficult. Changes to vertical distributions in response to environmental drivers (e.g., light) may occur on scales of 10s – 100s m which may have not been adequately captured in the present study.

4.3.2. Future Considerations

The reported deepening of vertical distributions and reduced/subdued DVM rates in the examined taxa within the LC and LCEs have the potential to alter the biological carbon pump in the northern GoM with potential reductions in carbon sequestration. Modeling of carbon transport in warm core eddies near Australia noted that reduced DVM rates within "warm core eddies" resulted in lower overall carbon flux out of the epipelagic (Kwong et al., 2020). Due to the highly transient nature of the LC and LCEs the potential magnitude is unknown and would require further exploration. However, given that acoustic surveys suggest that this pattern may be persistent across the GoM's mesopelagic fish assemblage there may be a large impact on the region's ability to sequester carbon in these LC affected regions that should be considered in future studies of carbon transport in the GoM (Boswell et al., 2020; Zimmerman and Biggs, 1999).

A notable mesoscale feature that was not examined in this study was cyclonic eddies (CEs) since they were not sampled during the timeframe of the study. CEs would potentially have the inverse effect as LCEs on carbon export due to potentially elevated rates of DVM and a shallower

mixed layer which could offset the effects of potentially shallower daytime distributions. CEs have the potential to offset the effects of the LC and LCEs on carbon transport though as discussed above further research to quantify the magnitude of the impact LC, LCEs, and CEs have on carbon transport is required to confirm this. Additionally, investigation of CEs may help clarify the drivers behind the structuring patterns observed in this study.

Another thing to consider is that while this study primarily looked at trawls from May to August the potential impact mesoscale eddies have on mesopelagic fish biomass patterns can vary seasonally. In subtropical gyres and in the GoM, anticyclonic eddies are shown to have increased total Chl-*a* in the wintertime when compared to surrounding water masses and cyclonic eddies (Damien et al., 2021; Dufois et al., 2016; Gaube et al., 2019; Siegel et al., 2011). This enhanced productivity is due to a combination of the deeper mixed layers generally found within anticyclonic eddies and enhanced convective mixing in the winter (Damien et al., 2021; Dufois et al., 2016). This results in nutrient rich waters being transported up into the euphotic zone during the winter which stimulates production (Damien et al., 2021; Dufois et al., 2016). Future studies should consider the lifetime of LCEs especially as their presumed effects diminish, as their impact on mesopelagic fish structuring may be altered during an eddy's lifetime.

Given the species-specific responses to the mesoscale features examined, future studies should consider modeling further taxa. A notable group that was not included in this study was the order Myctophiformes. Myctophiformes are the second most abundant order in the GoM making up around 15% of the catch in recent surveys and make up a significant part of the diel vertically migrating portion of the mesopelagic assemblage (Sutton et al., 2017b). Alterations to the Myctophid assemblage would likely have large impacts on carbon sequestration and also higher trophic level organisms. Additionally, the family Sternoptychidae was notably left out of this study but could be included in future studies due to their large abundance in the northern GoM and DVM behavior. Investigating further species of Cyclothone (e.g., *Cyclothone obsura*) may be considered as well due in part to their large biomass in the northern GoM and the relatively small number of studies investigating their distribution patterns and potential ecological significance.

5. Conclusion

The results of this study showed that stomiiform fishes largely display species-specific responses to mesoscale oceanographic features at the temporal and spatial scales examined. The most widespread and consistent trend across taxa was the alteration of vertical distributions as a function of water mass. The horizontal distribution of stomiiform fishes were marginally affected by the environmental variables examined with some exceptions in the cases of *S. elongatus* (Chl-*a*) and *P. guernei* (distance to nearest 200-m isobath). This project additionally hints at potential alterations of the biological carbon pump in the confines of the LC and its associated eddies that need to be considered in further studies of regional carbon transport. Ultimately further sampling is required particularly within these mesoscale features (e.g., LC and LCEs) to confirm many of the distribution patterns observed. The inclusion of *in situ* light measurements, further sampling of mesoscale features, and the inclusion of more taxa may help in disentangling the potential drivers of the spatial structuring observed and determine if these patterns can be generalized to the entire northern GoM mesopelagic assemblage.

References

Aguilar-Medrano, R., & Vega-Cendejas, M. E. (2020). Implications of the depth profile on the functional structure of the fish community of the Perdido Fold Belt, Northwestern Gulf of Mexico. *Reviews in Fish Biology and Fisheries*, *30*(4), 657-680. doi: 10.1007/s11160-020-09615-x

Aksnes, D. L., Røstad, A., Kaartvedt, S., Martinez, U., Duarte, C. M., & Irigoien, X. (2017). Light penetration structures the deep acoustic scattering layers in the global ocean. *Science Adv*ances, *3*(5). doi: 10.1126/sciadv.1602468

Bakun, A. (2006). Fronts and eddies as key structures in the habitat of marine fish larvae: Opportunity, adaptive response and competitive advantage. *Scientia Marina*, *70*(2), 105-122. doi: 10.3989/scimar.2006.70s2105

Bandara, K., Varpe, Ø., Wijewardene, L., Tverberg, V., & Eiane, K. (2021). Two hundred years of zooplankton vertical migration research. *Biological Reviews*, *96*(4), 1547-1589. doi: 10.1111/brv.12715

Bangma, J. L., & Haedrich, R. L. (2008). Distinctiveness of the mesopelagic fish fauna in the Gulf of Mexico. *Deep Sea Research Part II: Topical Studies in Oceanography*, *55*(24), 2594-2596. doi: 10.1016/j.dsr2.2008.07.008

Béhagle, N., du Buisson, L., Josse, E., Lebourges-Dhaussy, A., Roudaut, G., & Ménard, F. (2014). Mesoscale features and micronekton in the Mozambique Channel: An acoustic approach. *Deep Sea Research Part II: Topical Studies in Oceanography*, *100*, 164. doi: 10.1016/j.dsr2.2013.10.024

Belkin, I. M., Cornillon, P. C., & Sherman, K. (2009). Fronts in Large Marine Ecosystems. *Progress in Oceanography*, *81*(1), 223-236. doi: 10.1016/j.pocean.2009.04.015

Benoit-Bird, K. J., & Au, W. W. L. (2004). Diel migration dynamics of an island-associated sound-scattering layer. *Deep Sea Research Part I: Oceanographic Research Papers*, *51*(5), 707-719. doi: 10.1016/j.dsr.2004.01.004

Biggs, D. C. (1992). Nutrients, plankton, and productivity in a warm-core ring in the western Gulf of Mexico. *Journal of Geophysical Research: Oceans*, *97*(C2), 2143-2154. doi: 10.1029/90JC02020

Biggs, D. C., & Ressler, P. H. (2001). Distribution and abundance of phytoplankton, zooplankton, ichthyoplankton, and micronekton in the deepwater Gulf of Mexico. *Gulf of Mexico Science*, *19*(1), 2. doi: 10.18785/goms.1901.02

Bortoluzzo, A. B., Claro, D. P., Caetano, M. A. L., & Artes, R. (2011). Estimating total claim size in the auto insurance industry: a comparison between tweedie and zero-adjusted inverse gaussian distribution. *BAR-Brazilian Administration Review, 8*, 37-47.

Boswell, K. M., D'Elia, M., Johnston, M. W., Mohan, J. A., Warren, J. D., Wells, R. J. D., & Sutton, T. T. (2020). Oceanographic Structure and Light Levels Drive Patterns of Sound Scattering Layers in a Low-Latitude Oceanic System. *Frontiers in Marine Science*, *7*(51). doi: 10.3389/fmars.2020.00051

Butler, M., Bollens, S. M., Burkhalter, B., Madin, L. P., & Horgan, E. (2001). Mesopelagic fishes of the Arabian Sea: distribution, abundance and diet of Chauliodus pammelas, Chauliodus sloani, Stomias affinis, and Stomias nebulosus. *Deep Sea Research Part II: Topical Studies in Oceanography*, *48*(6), 1369-1383. doi: 10.1016/S0967-0645(00)00143-0

Cardona, Y., & Bracco, A. (2016). Predictability of mesoscale circulation throughout the water column in the Gulf of Mexico. *Deep Sea Research Part II: Topical Studies in Oceanography*, *129,* 332-349. doi: 10.1016/j.dsr2.2014.01.008

Chi, A., Vega-Cendejas, M. E., & Santillana, J. (2023). Length–weight relations of 39 continental-shelf and deep-water fishes (Actinopterygii) from northwestern Gulf of México. *Acta Ichthyologica et Piscatoria*, *53,* 59-64. doi: 10.3897/aiep.53.101788

Cook, A. B., Bernard, A. M., Boswell, K. M., Bracken-Grissom, H., D'Elia, M., deRada, S., Easson, C. G., English, D., Eytan, R. I., Frank, T., Hu, C., Johnston, M. W., Judkins, H., Lembke, C., Lopez, J. V., Milligan, R. J., Moore, J. A., Penta, B., Pruzinsky, N. M., Sutton, T. T. (2020). A Multidisciplinary Approach to Investigate Deep-Pelagic Ecosystem Dynamics in the Gulf of Mexico Following Deepwater Horizon. *Frontiers in Marine Science*, *7*(1122). doi: 10.3389/fmars.2020.548880

Cummings, J. A. (1984). Habitat dimensions of calanoid copepods in the western Gulf of Mexico. *Journal of Marine Research*, *42*(1), 163-188. doi: 10.1357/002224084788506121

Dagg, M. J., & Breed, G. A. (2003). Biological effects of Mississippi River nitrogen on the northern Gulf of Mexico—a review and synthesis. *Journal of Marine Systems*, *43*(3), 133-152. doi: 10.1016/j.jmarsys.2003.09.002

Damien, P., Sheinbaum, J., Pasqueron de Fommervault, O., Jouanno, J., Linacre, L., & Duteil, O. (2021). Do Loop Current eddies stimulate productivity in the Gulf of Mexico? *Biogeosciences*, *18*(14), 4281-4303. doi: 10.5194/bg-18-4281-2021

Davis, A. L., Sutton, T. T., Kier, W. M., & Johnsen, S. (2020). Evidence that eye-facing photophores serve as a reference for counterillumination in an order of deep-sea fishes. *Proceedings of the Royal Society B: Biological Sciences*, *287*(1928), 20192918. doi:10.1098/rspb.2019.2918

Davison, P. (2011). The specific gravity of mesopelagic fish from the northeastern Pacific Ocean and its implications for acoustic backscatter. *ICES Journal of Marine Science*, *68*(10), 2064-2074. doi: 10.1093/icesjms/fsr140

Davison, P. C., Checkley, D. M., Koslow, J. A., & Barlow, J. (2013). Carbon export mediated by mesopelagic fishes in the northeast Pacific Ocean. *Progress in Oceanography*, *116,* 14-30. doi: 10.1016/j.pocean.2013.05.013

Dawidowicz, P., & Pijanowska, J. (2018). Diel vertical migration of aquatic crustaceans—adaptive role, underlying mechanisms, and ecosystem consequences. *The Natural History of the Crustacea: Life Histories*, *22*, 231-256.

Della Penna, A., & Gaube, P. (2020). Mesoscale Eddies Structure Mesopelagic Communities. *Frontiers in Marine Science*, *7*(454). doi: 10.3389/fmars.2020.00454

Devine, B., Fennell, S., Themelis, D., & Fisher, J. A. D. (2021). Influence of anticyclonic, warm-core eddies on mesopelagic fish assemblages in the Northwest Atlantic Ocean. *Deep Sea Research Part I: Oceanographic Research Papers*, *173,* 103555. doi: 10.1016/j.dsr.2021.103555

Di Lorenzo, M., Calò, A., Di Franco, A., Milisenda, G., Aglieri, G., Cattano, C., Milazzo, M., & Guidetti, P. (2022). Small-scale fisheries catch more threatened elasmobranchs inside partially protected areas than in unprotected areas. *Nature Communications*, *13*(1), 4381. doi: 10.1038/s41467-022-32035-3

Dinnel, S. P., & Wiseman, W. J. (1986). Fresh water on the Louisiana and Texas shelf. *Continental Shelf Research*, *6*(6), 765-784. doi: 10.1016/0278-4343(86)90036-1

Dornan, T., Fielding, S., Saunders, R. A., & Genner, M. J. (2019). Swimbladder morphology masks Southern Ocean mesopelagic fish biomass. *Proceedings of the Royal Society B: Biological Sciences*, *286*(1903), 20190353. doi:10.1098/rspb.2019.0353

Drazen, J. C., De Forest, L. G., & Domokos, R. (2011). Micronekton abundance and biomass in Hawaiian waters as influenced by seamounts, eddies, and the moon. *Deep Sea Research Part I: Oceanographic Research Papers*, *58*(5), 557-566. doi: 10.1016/j.dsr.2011.03.002

Dufois, F., Hardman-Mountford, N. J., Greenwood, J., Richardson, A. J., Feng, M., & Matear, R. J. (2016). Anticyclonic eddies are more productive than cyclonic eddies in subtropical gyres because of winter mixing. *Science Advances*, *2*(5), e1600282. doi: 10.1126/sciadv.1600282

Duhamel, G., Koubbi, P., & Ravier, C. (2000). Day and night mesopelagic fish assemblages off the Kerguelen Islands (Southern Ocean). *Polar Biology*, *23*(2), 106-112. doi: 10.1007/s003000050015

Eden, B. R., Steinberg, D. K., Goldthwait, S. A., & McGillicuddy, D. J. (2009). Zooplankton community structure in a cyclonic and mode-water eddy in the Sargasso Sea. *Deep Sea Research Part I: Oceanographic Research Papers*, *56*(10), 1757-1776. doi: 10.1016/j.dsr.2009.05.005

Eduardo, L. N., Lucena-Frédou, F., Mincarone, M. M., Soares, A., Le Loc'h, F., Frédou, T., Ménard, F., & Bertrand, A. (2020). Trophic ecology, habitat, and migratory behaviour of the viperfish *Chauliodus sloani* reveal a key mesopelagic player. *Scientific reports*, *10*(1), 20996. doi: 10.1038/s41598-020-77222-8

Eilers, P. H., & Marx, B. D. (1996). Flexible smoothing with B-splines and penalties. *Statistical science*, *11*(2), 89-121.

Elliott, B. A. (1982). Anticyclonic Rings in the Gulf of Mexico. *Journal of Physical Oceanography*, *12*(11), 1292-1309. doi: 10.1175/15200485

Enea, M., Stasinopoulos, M., Rigby, B., & Hossain, A. (2019). gamlss. inf: Fitting mixed (inflated and adjusted) distributions [R package](Version 1.0-1.1). In.

Fennell, S., & Rose, G. (2015). Oceanographic influences on Deep Scattering Layers across the North Atlantic. *Deep Sea Research Part I: Oceanographic Research Papers*, *105*, 132-141. doi: 10.1016/j.dsr.2015.09.002

Frank, T., & Widder, E. (2002). Effects of a decrease in downwelling irradiance on the daytime vertical distribution patterns of zooplankton and micronekton. *Marine Biology*, *140*(6), 1181-1193. doi:10.1007/s00227-002-0788-7

Froese, R. (2006). Cube law, condition factor and weight–length relationships: history, meta-analysis and recommendations. *Journal of Applied Ichthyology*, *22*(4), 241-253. doi: 10.1111/j.1439-0426.2006.00805.x

Gartner Jr, J. V., Hopkins, T., Baird, R. C., & Milliken, D. (1987). The lanternfishes(Pisces: Myctophidae) of the eastern Gulf of Mexico. *Fishery Bulletin*, *85*(1), 81-98.

Gartner, J. V., Sulak, K. J., Ross, S. W., & Necaise, A. M. (2008). Persistent near-bottom aggregations of mesopelagic animals along the North Carolina and Virginia continental slopes. *Marine Biology*, *153*(5), 825-841. doi: 10.1007/s00227-007-0855-1

Gaube, P., J., McGillicuddy Jr., D., & Moulin, A. J. (2019). Mesoscale eddies modulate mixed layer depth globally. *Geophysical Research Letters*, *46*(3), 1505-1512. doi: 10.1029/2018GL080006

General Bathymetric Chart of the Ocean (GEBCO). (2023). British Oceanographic Data Centre. https://www.gebco.net

Genin, A. (2004). Bio-physical coupling in the formation of zooplankton and fish aggregations over abrupt topographies. *Journal of Marine Systems*, *50*(1), 3-20. doi: 10.1016/j.jmarsys.2003.10.008

Gierach, M. M., Vazquez-Cuervo, J., Lee, T., & Tsontos, V. M. (2013). Aquarius and SMOS detect effects of an extreme Mississippi River flooding event in the Gulf of Mexico. *Geophysical Research Letters*, *40*(19), 5188-5193. doi: 10.1002/grl.50995

Gjøsæter, J., & Kawaguchi, K. (1980). *A review of the world resources of mesopelagic fish FAO fishieries technical paper no. 193*. Food and Agriculture Organization of the United Nations, 1–151.
https://archive.org/details/reviewoftheworld034721mbp/page/n1/mode/1up

Godø, O. R., Samuelsen, A., Macaulay, G. J., Patel, R., Hjøllo, S. S., Horne, J., Kaartvedt, S., & Johannessen, J. A. (2012). Mesoscale eddies are oases for higher trophic marine life. *PLoS One*, *7*(1), e30161. doi: 10.1371/journal.pone.0030161

Goldthwait, S. A., & Steinberg, D. K. (2008). Elevated biomass of mesozooplankton and enhanced fecal pellet flux in cyclonic and mode-water eddies in the Sargasso Sea. *Deep Sea Research Part II: Topical Studies in Oceanography*, *55*(10), 1360-1377.
doi: 10.1016/j.dsr2.2008.01.003

Greenlaw, C. F., & Pearcy, W. G. (1985). Acoustical patchiness of mesopelagic micronekton. *Journal of Marine Research*, *43*, 163-178. doi: 10.1357/002224085788437352

Grieb, T. M., Donn, T. E., Collins, J., Radde, J., Perez, C., Smith, J. B., Rowe, G., Scott, S., & Ririe, G. (2008). *Effects of subsea processing on deepwater environments in the Gulf of Mexico*. U.S. Department of the interior minerals management service Gulf of Mexico OCS Region 5. https://info.publicintelligence.net/DeepwaterProcessing.pdf

Grimaldo, E., Grimsmo, L., Alvarez, P., Herrmann, B., Møen Tveit, G., Tiller, R., Slizyte, R., Aldanondo, N., Guldberg, T., Toldnes, B., Carvajal, A., Schei, M., & Selnes, M. (2020). Investigating the potential for a commercial fishery in the Northeast Atlantic utilizing mesopelagic species. *ICES Journal of Marine Science*, *77*(7-8), 2541-2556.
doi: 10.1093/icesjms/fsaa114

Gruber, B. (2009). [Review of the book Mixed effect models and extensions in ecology with R, by A.F. Zuur, E.N. Ieno, N.J. Walker, A.A. Saveliev & G.M. Smith]. Basic and Applied Ecology, 10(6), 588. doi: 10.1016/j.baae.2009.06.001

Heller, G. Z., Mikis Stasinopoulos, D., Rigby, R. A., & De Jong, P. (2007). Mean and dispersion modelling for policy claims costs. *Scandinavian Actuarial Journal*, *2007*(4), 281-292.

Herring, H. (2010). *Gulf of Mexico hydrographic climatology and method of synthesizing subsurface profiles from the satellite sea surface height anomaly*. US. Department of Commerce. National Oceanic and Atmospheric Administration. National Ocean Service. Coastal Survey Development Laboratory.
https://geo.gcoos.org/data/ssha/sshatsproflies.pdf

Hidalgo, M., & H. I. Browman (2019). Developing the knowledge base needed to sustainably manage mesopelagic resources. *ICES Journal of Marine Science 76*(3), 609-615. doi: 10.1093/icesjms/fsz067

Irigoien, X., Klevjer, T. A., Røstad, A., Martinez, U., Boyra, G., Acuña, J. L., Bode, A., Echevarria, F., Gonzalez-Gordillo, J. I., Hernandez-Leon, S., Agusti, S., Aksnes, D. L., Duarte, C. M., & Kaartvedt, S. (2014). Large mesopelagic fishes biomass and trophic efficiency in the open ocean. *Nature Communications*, *5*(1), 3271. doi: 10.1038/ncomms4271

Johnston, M. W., Milligan, R. J., Easson, C. G., deRada, S., English, D. C., Penta, B., & Sutton, T. T. (2019). An empirically validated method for characterizing pelagic habitats in the Gulf of Mexico using ocean model data. *Limnology and Oceanography: Methods*, *17*(6), 362-375. doi: 10.1002/lom3.10319

Jonasson, P. M. (1972). Ecology and production of the profundal benthos in relation to phytoplankton in Lake Esrom. *Oikos*, *14*, 1-148.

Kaartvedt, S., Christiansen, S. and Titelman, J. (2023), Mid-summer fish behavior in a high-latitude twilight zone. *Limnology and Oceanography*, *68*, 1654-1669. doi: 10.1002/lno.12374

Kaartvedt, S., Langbehn, T. J., & Aksnes, D. L. (2019). Enlightening the ocean's twilight zone. *ICES Journal of Marine Science, 76*(4), 803-812. doi :10.1093/icesjms/fsz010

Kaartvedt, S., Røstad, A., & Aksnes, D. L. (2017). Changing weather causes behavioral responses in the lower mesopelagic. *Marine Ecology Progress Series*, *574*, 259-263. doi: 10.3354/meps12185

Kaartvedt, S., Røstad, A., & Klevjer, T. A. (2009). Sprat Sprattus sprattus can exploit low oxygen waters for overwintering. *Marine Ecology Progress Series*, *390*, 237-249. doi: 10.3354/meps08196

Kayama, M., & Ikeda, Y. (1975). Studies on the lipids of micronektonic fishes caught in Sagami and Suruga Bays, with special reference to their wax esters. *Journal of Japan Oil Chemists' Society*, *24*(7), 435-440.

Klevjer, T. A., Irigoien, X., Røstad, A., Fraile-Nuez, E., Benítez-Barrios, V. M., & Kaartvedt, S. (2016). Large scale patterns in vertical distribution and behaviour of mesopelagic scattering layers. *Scientific Reports*, *6*, 19873. doi: 10.1038/srep19873

Kwong, L. E., Henschke, N., Pakhomov, E. A., Everett, J. D., & Suthers, I. M. (2020). Mesozooplankton and micronekton active carbon transport in contrasting eddies. *Frontiers in Marine Science*, *6*. doi: 10.3389/fmars.2019.00825

Langbehn, T. J., Aksnes, D. L., Kaartvedt, S., Fiksen, Ø., & Jørgensen, C. (2019). Light comfort zone in a mesopelagic fish emerges from adaptive behaviour along a latitudinal gradient. *Marine Ecology Progress Series*, *623,* 161-174. doi: 10.3354/meps13024

Last, K. S., Hobbs, L., Berge, J., Brierley, A. S., & Cottier, F. (2016). Moonlight drives ocean-scale mass vertical migration of zooplankton during the Arctic winter. *Current Biology*, *26*(2), 244-251. doi: 10.1016/j.cub.2015.11.038

Lindo-Atichati, D., Bringas, F., Goni, G., Muhling, B., Muller-Karger, F., & Habtes, S. (2012). Varying mesoscale structures influence larval fish distribution in the northern Gulf of Mexico. *Marine Ecology Progress Series*, *463,* 245-257. doi: 10.3354/meps09860

López-Pérez, C., Olivar, M. P., Hulley, P. A., & Tuset, V. M. (2020). Length–weight relationships of mesopelagic fishes from the equatorial and tropical Atlantic waters: Influence of environment and body shape. *Journal of Fish Biology*, *96*(6), 1388-1398. doi: 10.1111/jfb.14307

Lüdecke, D. (2018). ggeffects: Tidy data frames of marginal effects from regression models. *Journal of Open Source Software*, *3*(26), 772.

Luo, J., Ortner, P. B., Forcucci, D., & Cummings, S. R. (2000). Diel vertical migration of zooplankton and mesopelagic fish in the Arabian Sea. *Deep Sea Research Part II: Topical Studies in Oceanography*, *47*(7), 1451-1473. doi: 10.1016/S0967-0645(99)00150-2

Maul, G. A., & Vukovich, F. M. (1993). The relationship between variations in the gulf of mexico loop current and straits of florida volume transport. *Journal of Physical Oceanography*, *23*(5), 785-796. doi: 10.1175/1520-0485(1993)023<0785:Trbvit>2.0.Co;2

Mazumder, S. K., Das, S. K., Bakar, Y., & Ghaffar, M. A. (2016). Effects of temperature and diet on length-weight relationship and condition factor of the juvenile Malabar blood snapper (Lutjanus malabaricus Bloch & Schneider, 1801). *Journal of Zhejiang University. Science. B*, *17*(8), 580. doi: 10.1631/jzus.B1500251

Meinert, C. R., Clausen-Sparks, K., Cornic, M., Sutton, T. T., & Rooker, J. R. (2020). Taxonomic richness and diversity of larval fish assemblages in the oceanic gulf of mexico: Links to oceanographic conditions. *Frontiers in Marine Science*, *7*(579). doi: 10.3389/fmars.2020.00579

Milligan, R. J., & Sutton, T. T. (2020). Dispersion overrides environmental variability as a primary driver of the horizontal assemblage structure of the mesopelagic fish family myctophidae in the northern gulf of mexico. *Frontiers in Marine Science*, *7*(15). doi: 10.3389/fmars.2020.00015

Mohan, J. A., Sutton, T. T., Cook, A. B., Boswell, K. M., & Wells, R. J. D. (2017). Influence of oceanographic conditions on abundance and distribution of post-larval and juvenile carangid fishes in the northern Gulf of Mexico. *Fisheries Oceanography*, *26*, 526-541. doi: 10.1111/fog.12214

Morey, S. L., Schroeder, W. W., O'Brien, J. J., & Zavala-Hidalgo, J. (2003). The annual cycle of riverine influence in the eastern Gulf of Mexico basin. *Geophysical Research Letters*, *30*(16). doi: 10.1029/2003GL017348

NASA Goddard Space Flight Center, Ocean Ecology Laboratory, Ocean Biology Processing Group. (2018). Moderate-Resolution Imaging Spectroradiometer (MODIS) Aqua Chlorophyll Data; 2018 Reprocessing [Data set]. NASA OB.DAAC, doi: 10.5067/AQUA/MODIS/L3M/CHL/2018.

Ogle, D., Doll, J., Wheeler, A., & Dinno, A. (2023). *FSA: Simple fisheries stock assessment methods*. https://fishr-core-team.github.io/FSA/

Olson, D. B., & Backus, R. H. (1985). The concentrating of organisms at fronts: A cold-water fish and a warm-core Gulf Stream ring. *Journal of Marine Research*, *43*(1), 113-137. doi: 10.1357/002224085788437325

Penna, A. D., Llort, J., Moreau, S., Patel, R. S., Kloser, R. J., Gaube, P., Strutton, P. G., & Boyd, P. W. (2021). The impact of a Southern Ocean cyclonic eddy on mesopelagic micronekton. *Earth and Space Science Open Archive*, *21*. doi:10.1002/essoar.10507935.1

Pinheiro, J., Bates, D., DebRoy, S., Sarkar, D., & R Core Team. (2021). *Nlme: linear and nonlinear mixed effects models*. https://CRAN.R-project.org/package=nlme

Proud, R., Cox, M. J., & Brierley, A. S. (2017). Biogeography of the global ocean's mesopelagic zone. *Current Biology*, *27*(1), 113-119. doi: 10.1016/j.cub.2016.11.003

Pruzinsky, N. M., Milligan, R. J., & Sutton, T. T. (2020). Pelagic habitat partitioning of late-larval and juvenile tunas in the oceanic gulf of mexico. *Frontiers in Marine Science, 7*(257). doi: 10.3389/fmars.2020.00257

Richards, W. J., McGowan, M. F., Leming, T., Lamkin, J., & Kelley, S. (1993). Larval fish assemblages at the loop current boundary in the gulf of mexico. *Bulletin of Marine Science*, *53*, 475-537.

Rigby, R. A., & Stasinopoulos, D. M. (2005). Generalized additive models for location, scale and shape. *Journal of the Royal Statistical Society Series C: Applied Statistics*, *54*(3), 507-554.

Rooker, J. R., Simms, J. R., Wells, R. J. D., Holt, S. A., Holt, G. J., Graves, J. E., & Furey, N. B. (2012). Distribution and habitat associations of billfish and swordfish larvae across mesoscale features in the gulf of mexico. *PLoS One*, *7*(4), e34180. doi: 10.1371/journal.pone.0034180

Saba, G. K., Burd, A. B., Dunne, J. P., Hernández-León, S., Martin, A. H., Rose, K. A., Salisbury, J., Steinberg, D. K., Trueman, C. N., Wilson, R. W., & Wilson, S. E. (2021). Toward a better understanding of fish-based contribution to ocean carbon flux. *Limnology and Oceanography*, *66*(5), 1639-1664. doi: 10.1002/lno.11709

Sabarros, P., Ménard, F., Lévénez, J.-J., Tew Kai, E., & Ternon, J.-F. (2009). Mesoscale eddies influence distribution and aggregation patterns of micronekton in the Mozambique Channel. *Marine Ecology-Progress Series*, *395*, 101-107. doi: 10.3354/meps08087

Samuelsen, A., Hjøllo, S. S., Johannessen, J. A., & Patel, R. (2012). Particle aggregation at the edges of anticyclonic eddies and implications for distribution of biomass. *Ocean Science*, *8*(3), 389-400. doi: 10.5194/os-8-389-2012

Saunders, R. A., Hill, S. L., Tarling, G. A., & Murphy, E. J. (2019). Myctophid fish (Family Myctophidae) are central consumers in the food web of the Scotia Sea (Southern Ocean). *Frontiers in Marine Science*, *6*, 530. doi: 10.3389/fmars.2019.00530

Schiller, R. V., Kourafalou, V. H., Hogan, P., & Walker, N. D. (2011). The dynamics of the Mississippi River plume: Impact of topography, wind and offshore forcing on the fate of plume waters. *Journal of Geophysical Research: Oceans*, *116*(C6). doi: 10.1029/2010JC006883

Siegel, D. A., Peterson, P., McGillicuddy Jr, D., Maritorena, S., & Nelson, N. (2011). Bio-optical footprints created by mesoscale eddies in the Sargasso Sea. *Geophysical Research Letters*, *38*(13). doi: 10.1029/2011GL047660

Song, Y., Wang, C., & Sun, D. (2022). Both dissolved oxygen and chlorophyll explain the large-scale longitudinal variation of deep scattering layers in the tropical pacific ocean. *Frontiers in Marine Science*, *9*. doi: 10.3389/fmars.2022.782032

St. John, M. A., Borja, A., Chust, G., Heath, M., Grigorov, I., Mariani, P., Martin, A. P., & Santos, R. S. (2016). A dark hole in our understanding of marine ecosystems and their services: perspectives from the mesopelagic community. *Frontiers in Marine Science*, 3. doi: 10.3389/fmars.2016.00031

Staby, A., & Salvanes, A. G. V. (2019). Mesopelagic fish. In J. K. Cochran, H. J. Bokuniewicz, & P. L. Yager (Eds.), *Encyclopedia of ocean sciences* (3rd ed., pp. 283-289). Academic Press. doi: 10.1016/B978-0-12-409548-9.11212-6

Strömberg, J. O., Spicer, J. I., Liljebladh, B., & Thomasson, M. A. (2002). Northern krill, Meganyctiphanes norvegica, come up to see the last eclipse of the millennium? *Journal of the Marine Biological Association of the United Kingdom*, *82*(5), 919-920. doi: 10.1017/S0025315402006367

Sturges, W., Lugo-Fernandez, A., & Shargel, M. D. (2005). Introduction to Circulation in the Gulf of Mexico. In W. Surges, A. Lugo-Fernandez, & M.D. Shargel (Eds.) *Circulation in the Gulf of Mexico: Observations and models* (Vol. 161, pp. 1-10). American Geopysical Union. doi: 10.1029/161GM02

Sutton, T. T. (2013). Vertical ecology of the pelagic ocean: Classical patterns and new perspectives. *Journal of Fish Biology*, *83*(6), 1508-1527. doi: 10.1111/jfb.12263

Sutton, T. T., M. R. Clark, D. C. Dunn, P. N. Halpin, A. D. Rogers, J. Guinotte, S. J. Bograd, M. V. Angel, J. A. A. Perez, K. Wishner, R. L. Haedrich, D. J. Lindsay, J. C. Drazen, A. Vereshchaka, U. Piatkowski, T. Morato, K. Błachowiak-Samołyk, B. H. Robison, K. M. Gjerde, A. Pierrot-Bults, P. Bernal, G. Reygondeau and M. Heino. (2017a). A global biogeographic classification of the mesopelagic zone. *Deep Sea Research Part I: Oceanographic Research Papers*, *126*, 85-102. doi: 10.1016/j.dsr.2017.05.006

Sutton, T. T., Cook, A. B., Moore, J. A., Frank, T., Judkins, H. L., Vecchione, M., Nizinski, M. S., & Youngbluth, M. J. (2017b). *Inventory of Gulf oceanic fauna data including species, weight, and measurements. Meg Skansi cruises from Jan. 25 - Sept. 30, 2011 in the Northern Gulf of Mexico*. [Data set]. Gulf of Mexico Research Initiative Information and Data Cooperative (GRIIDC), Harte Research Institute, Texas A&M University – Corpus Christi. doi: 10.7266/N7VX0DK2

Sutton, T.T., Frank, T., Judkins, H., Romero, I.C. (2020). As gulf oil extraction goes deeper, who is at risk? Community structure, distribution, and connectivity of the deep-pelagic fauna. In: Murawski, S., Ainsworth, C., Gilbert, S., Hollander, D., Paris, C., Schlüter, M., Wetzel, D. (Eds.), *Scenarios and responses to future deep oil spills* (pp. 403-418). Springer, Cham. doi: 10.1007/978-3-030-12963-7_24

Sutton, T. T., & Hopkins, T. L. (1996). Species composition, abundance, and vertical distribution of the stomiid (Pisces: Stomiiformes) fish assemblage of the Gulf of Mexico. *Bulletin of Marine Science*, *59*(3), 530-542. doi: 10.1007/BF00942102

Tao, B., Tian, H., Ren, W., Yang, J., Yang, Q., He, R., Cai, W., & Lohrenz, S. (2014). Increasing Mississippi river discharge throughout the 21st century influenced by changes in climate, land use, and atmospheric CO2. *Geophysical Research Letters*, *41*(14), 4978-4986. doi: 10.1002/2014GL06036

Tarling, G., Buchholz, F., & Matthews, J. B. L. (1999). The effect of lunar eclipse on the vertical migration behaviour of Meganyctiphanes norvegica (Crustacea: Euphausiacea) in the Ligurian Sea. *Journal of Plankton Research*, *21,* 1475-1488. doi: 10.1093/plankt/21.8.1475

Turchini, G. M., Ng, W.-K., & Tocher, D. R. (2010). *Fish oil replacement and alternative lipid sources in aquaculture feeds.* CRC Press. doi:10.1201/9781439808634

Vukovich, F. M. (1988). Loop Current boundary variations. *Journal of Geophysical Research: Oceans*, *93*(C12), 15585-15591. doi: 10.1029/JC093iC12p15585

Vukovich, F. M. (2007). Climatology of ocean features in the gulf of mexico using satellite remote sensing data. *Journal of Physical Oceanography*, *37*(3), 689-707. doi: 10.1175/jpo2989.1

Vukovich, F. M., & Maul, G. A. (1985). Cyclonic eddies in the eastern gulf of mexico. *Journal of physical oceanography*, *15*, 105. doi: 10.1175/1520-0485(1985)015<0105:Ceiteg >2.0.Co;2

Wang, V. H., Zapfe, C. R., & Hernandez, F. J. (2021). Assemblage structure of larval fishes in epipelagic and mesopelagic waters of the northern gulf of mexico. *Frontiers in Marine Science, 8*. doi: 10.3389/fmars.2021.766369

Wang, Z., Dimarco, S., Ingle, S., Belabbassi, L., & Al-Kharusi, L. (2014). Seasonal and annual variability of vertically migrating scattering layers in the northern Arabian Sea. *Deep Sea Research Part I: Oceanographic Research Papers*, *90*. doi: 10.1016/j.dsr.2014.05.008

Williams, A., Koslow, J. A., & Last, P. R. (2001). Diversity, density and community structure of the demersal fish fauna of the continental slope off western Australia (20 to 35 S). *Marine Ecology Progress Series*, *212*, 247-263. doi: 10.3354/meps212247

Wormuth, J. H., Ressler, P. H., Cady, R. B., & Harris, E. J. (2000). Zooplankton and micronekton in cyclones and anticyclones in the northeast Gulf of Mexico. *Gulf of Mexico Science*, *18*(1), 3. doi: 10.18785/goms.1801.03

Zimmerman, R. A., & Biggs, D. C. (1999). Patterns of distribution of sound-scattering zooplankton in warm- and cold-core eddies in the Gulf of Mexico, from a narrowband acoustic Doppler current profiler survey. *Journal of Geophysical Research: Oceans*, *104*(C3), 5251-5262. doi: 10.1029/1998JC900072

Zuur, A.F.I., Elena, N., Walker, Neil, J., Saveliev, Anatoly A., Smith, Graham M. (2009). *Mixed effects models and extensions in ecology with R.* Springer

Zuur, A. F., Ieno, E. N., & Elphick, C. S. (2010). A protocol for data exploration to avoid common statistical problems. *Methods in Ecology and Evolution*, *1*(1), 3-14. doi: 10.1111/j.2041-210X.2009.00001.x

Zhang, C., Chen, Y., Xu, B., Xue, Y., & Ren, Y. (2020). Improving prediction of rare species' distribution from community data. *Scientific Reports*, *10*(1), 12230. doi: 10.1038/s41598-020-69157-x

Zhang, Y., Hu, C., Barnes, B. B., Liu, Y., Kourafalou, V. H., McGillicuddy Jr., D. J., Cannizzaro, J. P., English, D. C., & Lembke, C. (2023). Bio-optical, physical, and chemical properties of a loop current eddy in the Gulf of Mexico. *Journal of Geophysical Research: Oceans*, *128*(3), e2022JC018726. doi: 10.1029/2022JC018726